RIVIERA WIND FARM EFFECT
ON
KINGSVILLE NAVAL AIR STATION RADAR

Written by	Checked by	Approved by
S. Yun, M. Rais	P. Missud	
ATDI	**ATDI**	

TABLE OF CONTENTS

1. ABBREVIATIONS 4

2. INTRODUCTION 5

   2.1 *Background* 5

   2.2 *Objective* 6

   2.3 *Executive Summary* 7

3. CARTOGRAPHIC DATA FOR COMPUTATIONS 9

4. WIND TURBINE LOS ANALYSIS 11

   4.1 *LOS analysis basics* 11

   4.2 *Minimum distance for turbines to be out of ATC radar line-of-sight* 12

   4.3 *Shadowing due to wind turbine in LOS* 15

5. WIND TURBINE REFLECTION EFFECT ANALYSIS 17

   5.1 *Wind turbine radio cross section* 17

   5.2 *Reflection due to wind turbine* 19

   5.3 *PSR antenna patterns* 20

   5.4 *PSR clutter return at 2785MHz operating frequency – low beam* 22

   5.5 *PSR clutter return at 2785 MHz operating frequency – high beam* 29

6. AGGREGATED WIND TURBINE EFFECTS 32

   6.1 *Number of wind turbines per resolution cell* 33

   6.2 *Resolution cells with likely target loss* 34

   6.3 *False targets caused by the 'twinkling' effect* 36

7. CONCLUSION 40

8. REFERENCES 41

9. APPENDIX 43

   A. *Table of PSR clutter returns* 43

LIST OF FIGURES

Figure 1: Cartography in HTZ Warfare 10
Figure 2: Image captured during Kingsville region site survey 11
Figure 3: Minimum LOS model 12
Figure 4: LOS from radar to nearest wind turbine (~9 nmi) 14
Figure 5: LOS path from radar to furthest wind turbine (~11.5 nmi) 14
Figure 6: Kingsville Radar LOS Coverage 15
Figure 7: Shadows caused by wind turbines and terrain 16
Figure 8: Kingsville DASR-11 Horizontal Antenna Pattern 20
Figure 9: Typical PSR Antenna Elevation Pattern Characteristics 21
Figure 10: Effects of radar antenna tilt on elevation radiation pattern 22
Figure 11: PSR windfarm clutter return simulation in HTZ Warfare 25
Figure 12: Clutter return from single wind turbine vs. radar azimuth (9 nmi) – low beam 27
Figure 13: Clutter return from single wind turbine vs. radar azimuth (11.5nmi) – low beam 28
Figure 14: Clutter return from single wind turbine vs. radar azimuth (9 nmi) – high beam 30
Figure 15: Clutter return from single wind turbine vs. radar azimuth (11.5 nmi) – high beam 31
Figure 16: Proposed location of wind farm and its azimuth with respect to the ASR-11 radar 32
Figure 17: Wind turbines within resolution cells 33
Figure 18: Resolution cells with possible target loss 34
Figure 19: Detail of resolution cells with possible target loss 35
Figure 20: Rings of possible false target plots 37
Figure 21: 60 nautical mile detection range of PSR 38

LIST OF TABLES

Table 1: Values for RCS calculation 17
Table 2: ASR-11 PSR specifications 23
Table 3: Clutter return to PSR at 2785 MHz – low beam 24
Table 4: Comparison of clutter returns from mathematical model and HTZ Warfare simulation – low beam 26
Table 5: Comparison of clutter returns from mathematical model and HTZ Warfare simulation - high beam 29
Table 6: Comparison of PSR clutter returns of mathematical model and HTZ Warfare simulation 43

1. Abbreviations

ASL	Above Sea Level
ATC	Air Traffic Control
CAA	Civil Aviation Authority
CAD	Computer Aided Design
CFAR	Constant False Alarm Rate
DASR	Digital Airport Surveillance Radar
I/N	Interference to Noise ratio
IEEE	Institute of Electrical and Electronics Engineers
ITU	International Telecommunication Union
ITU-R	ITU Radiocommunication Sector
LOS	Line of Sight
MCEB	Military Communications-Electronics Board
MSSR	Monopulse Secondary Surveillance Radar
MTD	Moving Target Detection
MTI	Moving Target Indication
NAS	Naval Air Station
NTIA	National Telecommunications and Information Administration
PCR	Pulse Compression Ratio
PSR	Primary Surveillance Radar
RCS	Radar Cross Section
RF	Radio Frequency
SFAF	Standard Frequency Action Format
Tx/Rx	Transmitter/ Receiver
USGS	US Geological Survey
WT	Wind Turbine

2. Introduction

2.1 Background

With a growth rate of nearly 32% for the year 2009 and forecasted for a sevenfold increase in overall electricity output over the next decade, wind farms are becoming a defining characteristic of landscapes the world over. Due to the large size and metallic construction of the wind turbines, they have the potential of creating interference for radar installations in the form of shadowing, target loss, and false target generation.

A plethora of mitigation techniques exist to combat the interference caused to air traffic control, or ATC, radars by wind turbines. They range from crude to highly complex. Simpler techniques involve the use of terrain screening and the tilting of the radar antenna so that the beam does not illuminate any wind turbines [1]. By utilizing the natural variations in terrain altitude, turbines are placed in a way as to prevent illumination by radar. In addition, by simply tilting the radar with respect to the horizon, illumination of turbines may be prevented, but at the expense of reduced detection for low-flying aircraft targets.

Further enhancements to the radar's processing algorithms may yield mitigation at the pre-detection, detection, and post-detection stages [2]. Azimuth gating electronically limits the detection range of the radar antenna for select azimuths, maintaining full detection range for all unaffected azimuths. Through modification of the radar's constant false alarm rate (CFAR) algorithm, shadowing caused by wind turbines is lessened during the detection stage. Enhanced tracking techniques are implemented at the post-detection stage.

Currently, studies are taking place regarding the application of stealth technologies to the wind turbines themselves [3]. Stealth technologies minimize the radio cross section, or RCS, footprint of the moving and nonmoving parts of the turbine. They range from altering the shape of the tower and nacelle to yield smoother surfaces to the use of radar absorbing materials in the construction and coating of both blades and towers. While the use of shaping can significantly reduce the radar signature of nonmoving parts, the rotating blades require application of costlier radar absorbing materials.

Finally, the use of gap-fill radars and mini-phased arrays placed within or near wind farms [4] has also been explored and advocated. Gap-fill radars have traditionally been deployed to monitor the gap airspace that is located between ATC radar units. Through gating of the main ATC radar, deployment of a gap-fill radar, and subsequent merging of the data obtained by the two, airspace is completely covered without interference introduced by the wind turbines being prevalent. X-band mini-phased array radar is a concept that Raytheon has recently invested in heavily, seeing it as potentially the best candidate for the mitigation of the adverse effects caused by wind turbines.

2.2 Objective

The objective of this report is to utilize the optimal cartographic data in ATDI's HTZ Warfare RF planning software to most efficiently analyze any potential interference effects of the projected wind turbines on the Raytheon DASR-11 radar located at Kingsville Naval Air Station, supported by theoretical calculations based on formulas from commonly available literature. The three scenarios below are considered to determine the effect of Riviera wind farm.

The three areas of focus that may lead to interference scenarios are:

- Turbines within radar line-of-sight
- Target loss due to high clutter return
- False target plots due to high clutter return

LOS analysis has to do with wind turbines obstructing the direct path between radar and target of interest – creating a shadow zone within which targets may be lost due to the degradation of the radar signal strength. Firstly, a mathematical approach is employed to determine whether the Riviera wind farm is within range and can thus potentially create a shadow zone. Once it is determined that a shadow zone is created, HTZ Warfare is used to geographically model the affected area. Given the curvature of the earth, a minimum distance is also calculated for which the wind farm would be completely out of range of the radar.

Reflection and scattering deal with the impact and subsequent deflection of energy when a radio wave illuminates a stationary object; in this case when a radar signal impacts the tower of a wind turbine and is reflected, potentially back into the receiver [5]. The reflection is examined in the sense of clutter return; the wind turbines are considered clutter, much like any unwanted buildings, terrain, or vegetation that may be within the path of transmitted radio signals. The magnitude of the radio waves reflected back into the receiver is considered and compared with the radar's sensitivity level, establishing whether the magnitude of the returns breaches that level and would have an impact on the performance of the system. The Doppler effect - caused due to speed of the turbine blades scattering energy that exceeds radar noise floor - is also considered.

Individual turbines are analyzed at first for potential target loss and false target plot scenarios. The proposed wind farm is then studied as a whole to determine worst-case scenario effects, whereupon the reflections from all wind turbines may cause significant radar performance degradation, reflecting enough energy to drown out energy reflections from actual airborne targets and potentially creating false targets on the radar display.

Further effects that cause radar performance degradation are possible. Multiple scatterings and overall noise level elevation are more than possible. Due to their highly variable parameters, though, they cannot be easily quantitatively analyzed and are thus not included in this report.

2.3 Executive Summary

The proposed Riviera Wind Farm near Riviera, Texas, is to be composed of 75 Vestas V90-1.8MW wind turbines. The wind farm is to be located between 9 and 11.5 nautical miles from the Raytheon DASR-11 primary surveillance radar in use by NAS Kingsville. Due to the proximity of the turbines and the radar, significant interference effects are possible that may inhibit safe air space operation.

Wind turbines add a large stationary element and a complex moving element to flat and geographically featureless landscapes like that of Kleberg County, Texas, the location of NAS Kingsville and the proposed Riviera Wind Farm. While the stationary element—the turbine tower—is a major concern due to its height that extends to hundreds of feet, the moving element—the turbine's nacelle and blades—add the greatest amount of uncertainty. As both wind speed and wind direction vary, so does the apparent radar footprint, or the radar cross section, of the wind turbine. At certain blade/nacelle orientations, a wind turbine appears 'larger' to radar than at others.

To analyze the impact of the proposed wind farm on the NAS Kingsville radar, a review of pertinent literature is conducted first. The review reveals a number of useful documents from both US and UK government agencies and some relevant papers from academia. Having established a background, the radio interference effects are calculated mathematically and using ATDI's HTZ Warfare RF planning tool for graphical and numerical analysis. Ultimately, three sources of radar performance degredation are the subject of investigation: shadowing, target loss, and false target generation.

Shadowing is the result of a turbine being in the line-of-sight between radar and an airborne target, thus obstructing the direct path between the two and producing a shadow region behind the turbine. As the electromagnetic energy emitted by radar impacts a turbine, it is scattered, leading to a volume of lesser energy behind the turbine. Due to this volume of diminished energy, it is possible for airborne targets to be hidden by an obstructing turbine, preventing their detection. Assuming strict adherence to the flight patterns near NAS Kingsville, though, the shadowing effect is not likely to cause significant operational restrictions. Minimum flight altitudes in the direction of the proposed wind farm range from 800 feet at 10 nautical miles from the radar to 3100 feet at 38 nautical miles from the radar. For the wind turbines to be out of the radar's line-of-sight (and thus for no possibility of shadowing or other adverse effects), they should be located 38 nmi away from the radar.

Target loss is the momentary or complete loss of an airborne target aircraft by radar. Target loss is likely to occur when aircraft are directly above or near the proposed wind farm due to the strong clutter returns from the turbines. Because of their large size, the electromagnetic energy reflected by wind turbines greatly surpasses that of the energy reflected by an aircraft when the two are at the same range and azimuth based on an assumed turbine RCS of 30 dBsm. Assuming a nominal resolution cell size for 0.8 Pd as stated in the Raytheon DASR-11 product manual, 114 resolution cells

out of approximately 2700 (given a detection range of 60 nautical miles for the radar) are potentially dominated by the energy returns from wind turbines. In these cells, it is unlikely that an aircraft will be detected. For 60 nmi of detection range, this corresponds to 0.07% of all cells and 0.057% of total detection area.

False targets are generated in numerous ways; wind turbines may generate false targets on the radar display because their moving parts impart a Doppler frequency shift onto reflected radio signals. This change in frequency potentially tricks radar processing algorithms into interpreting the turbines as moving targets. Based on the spacing of the wind turbines and wind speed and wind direction, wind turbines may appear to 'twinkle' on the radar display, appearing suddenly and for a short amount of time. Given the proximity of the proposed wind farm to the radar and the radar antenna's gain, false targets may appear anywhere within a ring of minimum radius 9 nmi and a maximum radius of 11.5 nmi from the radar. It is not possible to numerically describe this effect, other than the area where it will possibly occur.

Ultimately, the questions of 'how many wind turbines are permissible' and 'how close is too close' are determined by the operational needs at the affected radar site and the mitigation capabilities allowed by the installed radar system. The number of wind turbines closely correlates to the number of resolution cells effected, where turbine reflected energy signatures dominate those of target aircraft within a cell. The potential for false targets diminishes as turbines are moved further away from radar. At approximately 25 nautical miles from the radar, there is little potential for false target generation at any azimuth other than the main beam and side lobe of greatest gain.

It is important to note that other forms of electromagnetic interference caused by the wind turbines are possible. The amount of energy scattered by a wind farm is immense. The manner in which the energy is scattered is also random and unpredictable. Due to multiple scatterings between more than one turbine and multipath effects, further radar performance degradation may occur, including overall noise level increase in the vicinity of the wind farm.

3. Cartographic Data for Computations

ATDI's RF network modeling platform, HTZ Warfare, is a comprehensive RF communications software application for civil and military networks operating from 10 kHz up to 450 GHz. It can be configured by the user to be a specialist toolbox for network design, optimization, and validation. The platform offers a graphical map interface for local single user and networked planning teams.

HTZ Warfare uses digital terrain and clutter information from various sources including NASA SRTM, USGS NED and SDTS to define the modeling environment. The GeoData from these sources are converted to raster matrices in ATDI's proprietary format. This format can be defined in the following way:

- **Digital Terrain Model (.GEO):** Contains bald earth terrain altitudes.
  For this study, ATDI prepared a UTM (Universal Transverse Mercator) projected terrain tile to serve as the base workspace grid for modeling. The UTM coordinate system is a grid-based method of specifying locations on the surface of the Earth that is a practical application of a 2-dimensional Cartesian coordinate system.

- **Clutter Layer (.SOL):** Typically contains a 2D description of the above ground morphological conditions of a given environment. This is described as a series of values on a grid that refer to 'clutter codes' that are freely reinterpreted with propagation characteristics inside HTZ Warfare. For this study, the clutter file along with a code for wind turbine locations and its height were used to describe effective obstructions within the terrain.

- **Image Layer (.RIM/.PAL):** Contains the color code and imagery values that constitute a reference map whether it be a digitized paper map, satellite photo or aerial photo. For this study, ATDI created both USGS 1:24K Scale Digital Raster Graphics (DRG) map and 1 meter resolution USGS National Agriculture Imagery Program (NAIP). A DRG is a scanned image of a U.S. Geological Survey standard series topographic map, including all map collar information. The image inside the map neatline is georeferenced to the surface of the earth and fit to the UTM projection. The horizontal positional accuracy and datum of the DRG matches the accuracy and datum of the source map. NAIP is aerial imagery acquired during the agricultural growing seasons in the continental U.S.

Each of the above matrices are projected in a metric projection to allow HTZ Warfare to accurately perform calculations. The clutter and imagery matrices are overlaid on the terrain matrix with each layer containing distinct information relevant to calculating the path loss between any points on the map.

Below is an example of how the GeoData is loaded into HTZ Warfare after it is prepared in ATDI format:

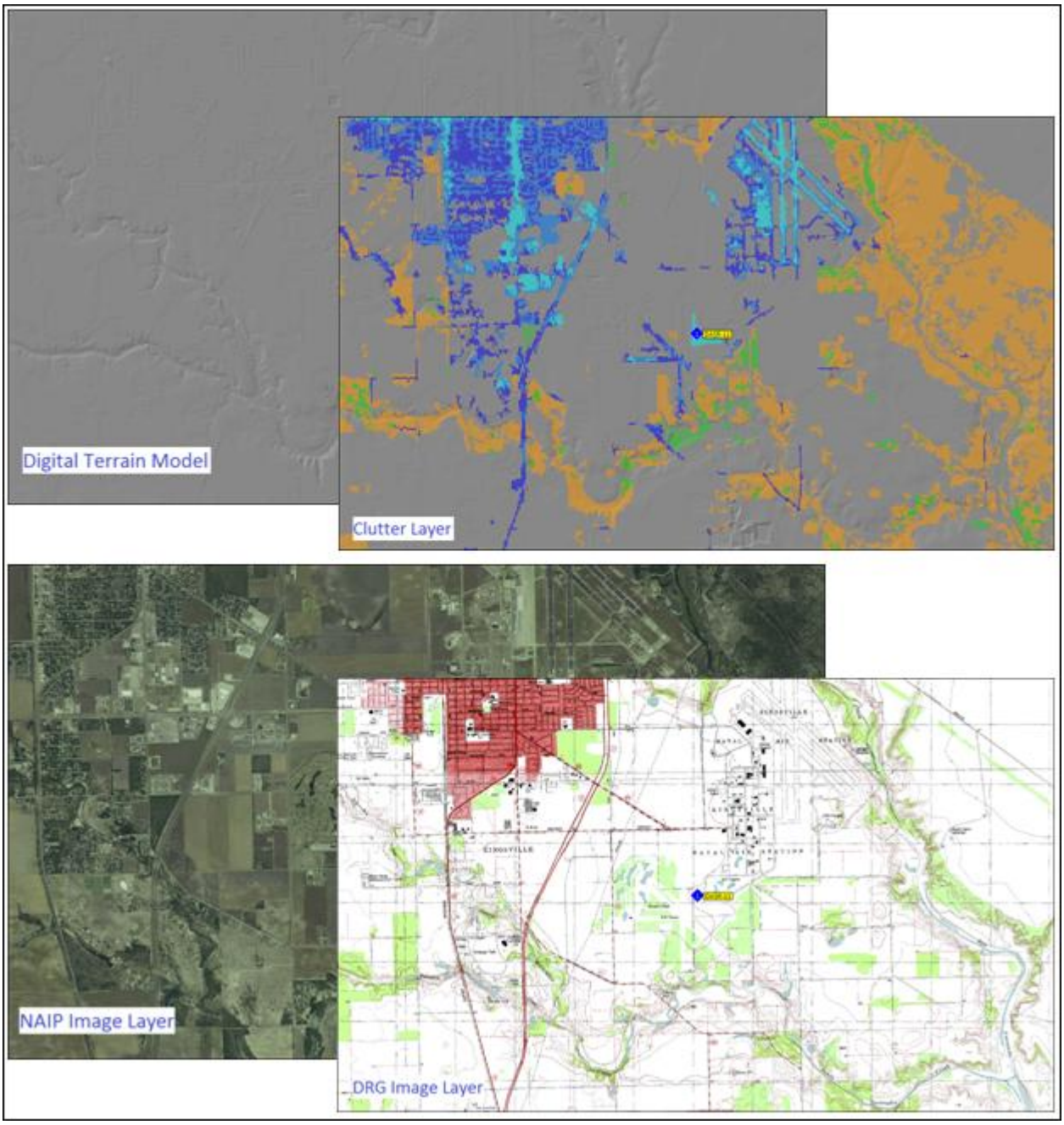

Figure 1: Cartography in HTZ Warfare

4. Wind Turbine LOS Analysis

4.1 LOS analysis basics

Line-of-sight is defined as an unobstructed path between two objects of arbitrary distance apart. That is, LOS is established when a wind turbine can be seen optically, by radio waves, or by both, from an ATC radar, and vice versa, with no geological formations, buildings, or vegetation completely obstructing the given path. The LOS path is also known as the radio path.

If it is deemed that a wind turbine is out of the LOS of the radar, there is no need for further analysis. The turbine may be deemed as out of the LOS of the radar when it is located at a great enough distance or when the LOS is obstructed so that radio waves do not impact upon its physical structure. Due to the curvature of the earth, when a turbine is located at a great enough distance, it will be hidden by the horizon, given smooth terrain. When a geological formation (usually of a greater elevation) is in the direct LOS between radar and a wind turbine, again the turbine is hidden from the radar, usually at a much shorter distance than due to the curvature of the earth. As can be seen in the image below, the terrain in Kleberg County, especially in the area where the Riviera Wind Farm is proposed, is mostly smooth with little elevation change. The image below was captured during the site visit to NAS Kingsville and the surrounding area.

Figure 2: Image captured during Kingsville region site survey

Somewhat greater care must be taken in LOS analysis, though, due to the phenomenon of diffraction. Diffraction allows for the bending of radio waves around materials so that they impact upon objects that are not optically visible from the radiating source [6]. By diffracting in the earth's atmosphere, radio waves bend around the earth's surface and can travel far beyond the visible horizon. Also, due to diffraction, the effective height of any geological formation in the direct line-of-sight is reduced in its effectiveness at preventing direct LOS. The amount the effective height is reduced is by the radius of the second Fresnel zone (the second Fresnel zone is considered in order to provide a more conservative, and realistic, approach toward modeling the varying characteristics of wind turbines) [5] of the transmitted radio waves. Thus, both an optical shielding point and a radar shielding point are obtained [7], though the radar shielding point is the only one of real interest.

Line-of-sight calculations are preformed in the following section. If a wind turbine is deemed to be within radio LOS of the ATC radar, its presence may have adverse effects on the radar's performance. Most notably, it may yield an increase in the radar's effective noise floor level through reflection.

4.2 Minimum distance for turbines to be out of ATC radar line-of-sight

Through a simple mathematical model, it is possible to establish a maximum LOS distance between the radar installation and any wind turbines in its vicinity based on the curvature of the earth and the assumption of smooth terrain. That is, we are interested in establishing a minimum distance between the ATC radar and any one wind turbine such that a radio signal transmitted from either location is not incident upon the other. The model detailed herein is based upon NTIA Technical Report TR-08-454 [8]. The figure below offers a basic diagram of the situation.

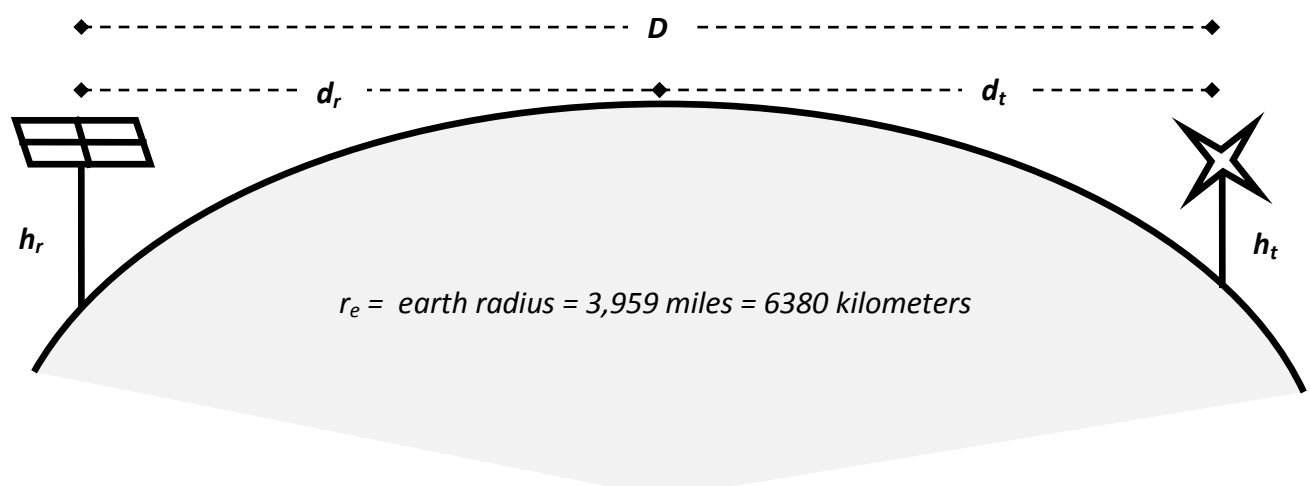

Figure 3: Minimum LOS model

where

D is the total distance between the ASR-11 radar and a wind turbine (mi)
d_r is the distance from the radar to the radio horizon (mi)
d_t is the distance from the wind turbine to the radio horizon (mi)
h_r is the height of the radar (ft)
h_t is the height of the wind turbine (ft)
r_e is the radius of the earth (mi)

In the calculations, one accounts for atmospheric diffraction effects by using the earth's effective radius, which is 4/3 times its actual radius in most circumstances. This factor accounts for the bending of radio signals around the earth's horizon, allowing them to travel greater distances than optical LOS. Thus, the distance between either of the objects and the horizon can be calculated using a simplified version of the Pythagorean Theorem:

$$d_r \approx \sqrt{2 * \frac{4}{3} r_e * h_r}$$
$$d_t \approx \sqrt{2 * \frac{4}{3} r_e * h_t} \qquad (1)$$

The height of the radar is 94 feet above mean sea level. Though the wind turbines vary in mean height above sea level, the tallest turbine is chosen for analysis because it will provide for a worst-case scenario; the tallest turbine is 451 feet above mean sea level. Combining the two distances, one solves for the overall minimum distance for non-LOS:

$$D = d_r + d_t = \sqrt{2 * \frac{4}{3}(5280 * 3959) * 94} + \sqrt{2 * \frac{4}{3}(5280 * 3959) * 451}$$
$$D = 2.31 * 10^5 ft = \mathbf{43.74\ mi = 38\ nmi} \qquad (2)$$

Thus, assuming flat earth, if the wind turbines are all located at a distance greater than 38 nautical miles from the ATC radar, no adverse effects to the radar's performance are to be expected. This is not the case, though, as all 75 turbines of the Riviera wind farm are to be 9 to 11.5 nautical miles away from the ATC radar at Kingsville NAS, well within the 38 nautical mile boundary. The two figures below show the direct line-of-sight from the radar to the nearest (~9 nmi) and then furthest (~11.5 nmi) wind turbines. The LOS path is denoted by the straight green line while the blue oval represents the first Fresnel zone of the radio signal. The figures were generated in ATDI's HTZ Warfare software.

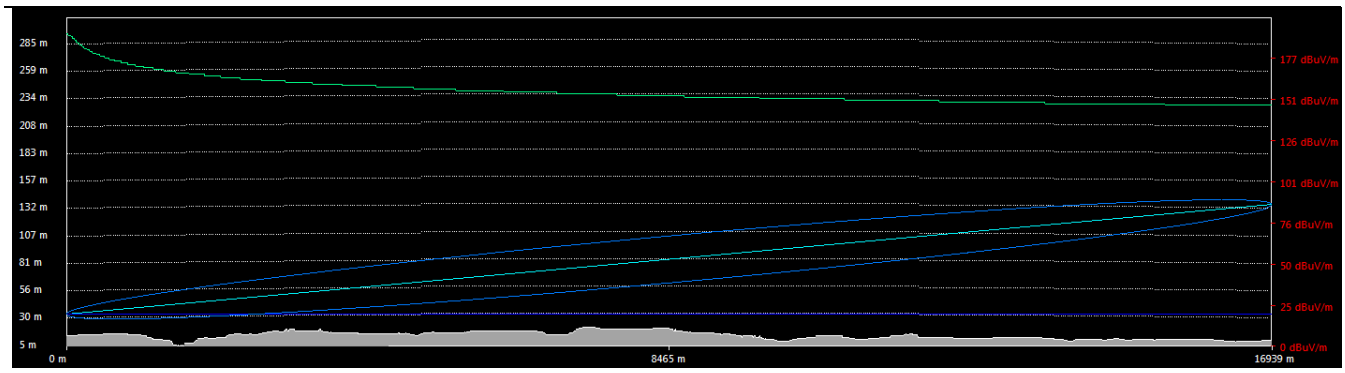

Figure 4: LOS from radar to nearest wind turbine (~9 nmi)

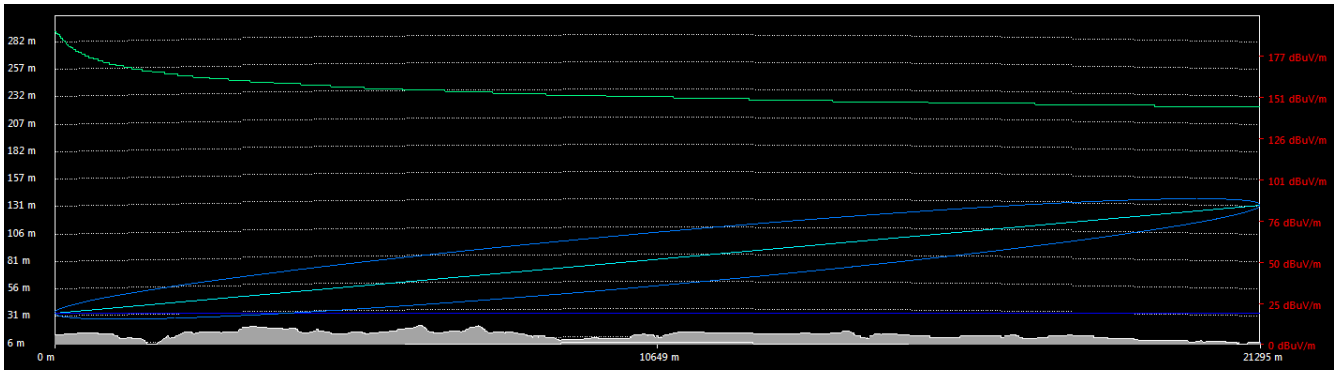

Figure 5: LOS path from radar to furthest wind turbine (~11.5 nmi)

Including the first Fresnel zone clearance and terrain data, the radar's maximum LOS distance to the wind farm is 22.4 nmi.

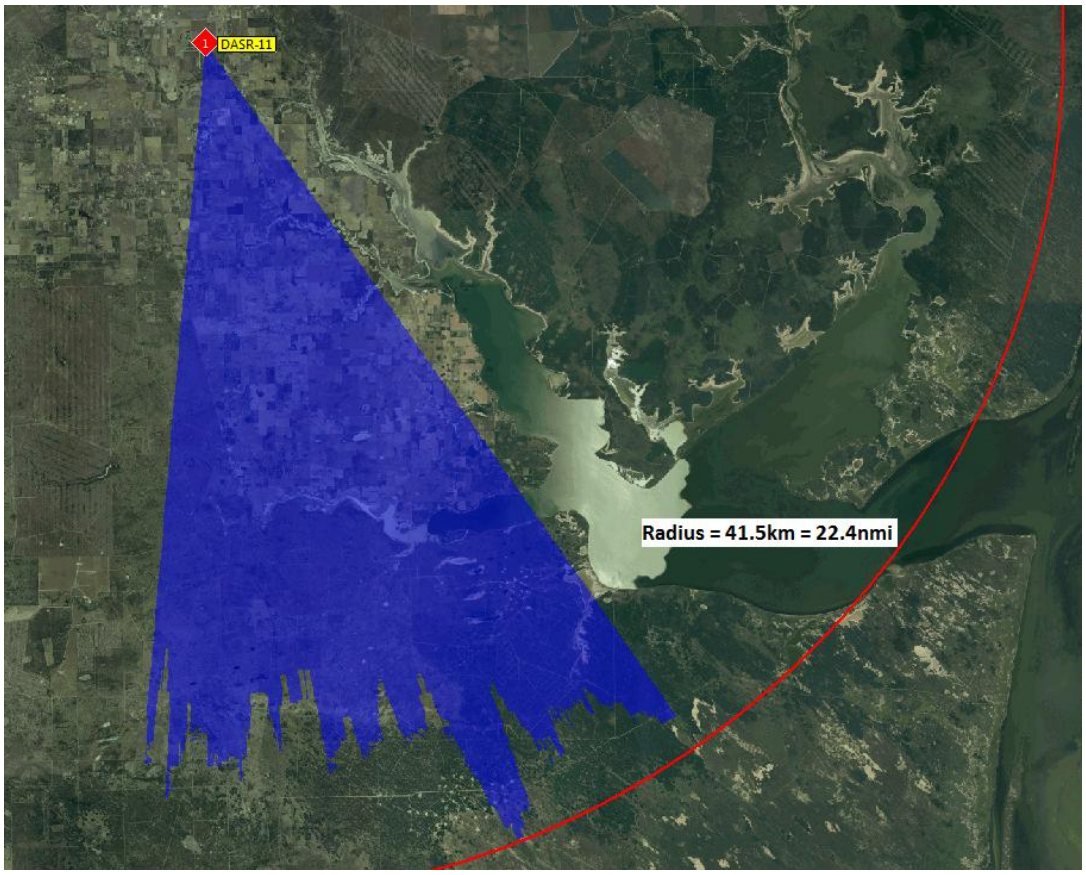

Figure 6: Kingsville Radar LOS Coverage

4.3 Shadowing due to wind turbine in LOS

Since the turbines are located within the line-of-sight distance of the radar, they can produce shadows behind themselves. These three-dimensional shadows appear in the form of narrow wedges when viewed from both a top view and a side view, stretching for many miles beyond the blocking turbine. Targets of interest may be lost within such a shadow due to the reduced field strength of the radar signal since the full power of the transmitted signal does not penetrate beyond the blocking wind turbines.

The figure below shows the shadowing effect caused by wind turbines (red dots) in radar's line-of-sight with various flight altitude requirements for the area. The bottom of the map is approximately 38 nautical miles from the radar location. The minimum flight altitude requirement would be 950 meter (3100 ft) at this distance (approximately 38 nmi away) in order to be above the shadow zone.

At a distance of 5 nautical miles from the ATC radar, the flight paths for the Naval Air Station dictate a flight altitude of 1800 feet. An aircraft would have to be at a distance of 26 nautical miles or more from the radar at this flight altitude to be in peril of being in the shadow region of a wind turbine. Thus, the Riviera wind farm should not cause LOS issues for departing and approaching aircraft that adhere to the flight patterns dictated for takeoff and landing at Kingsville NAS.

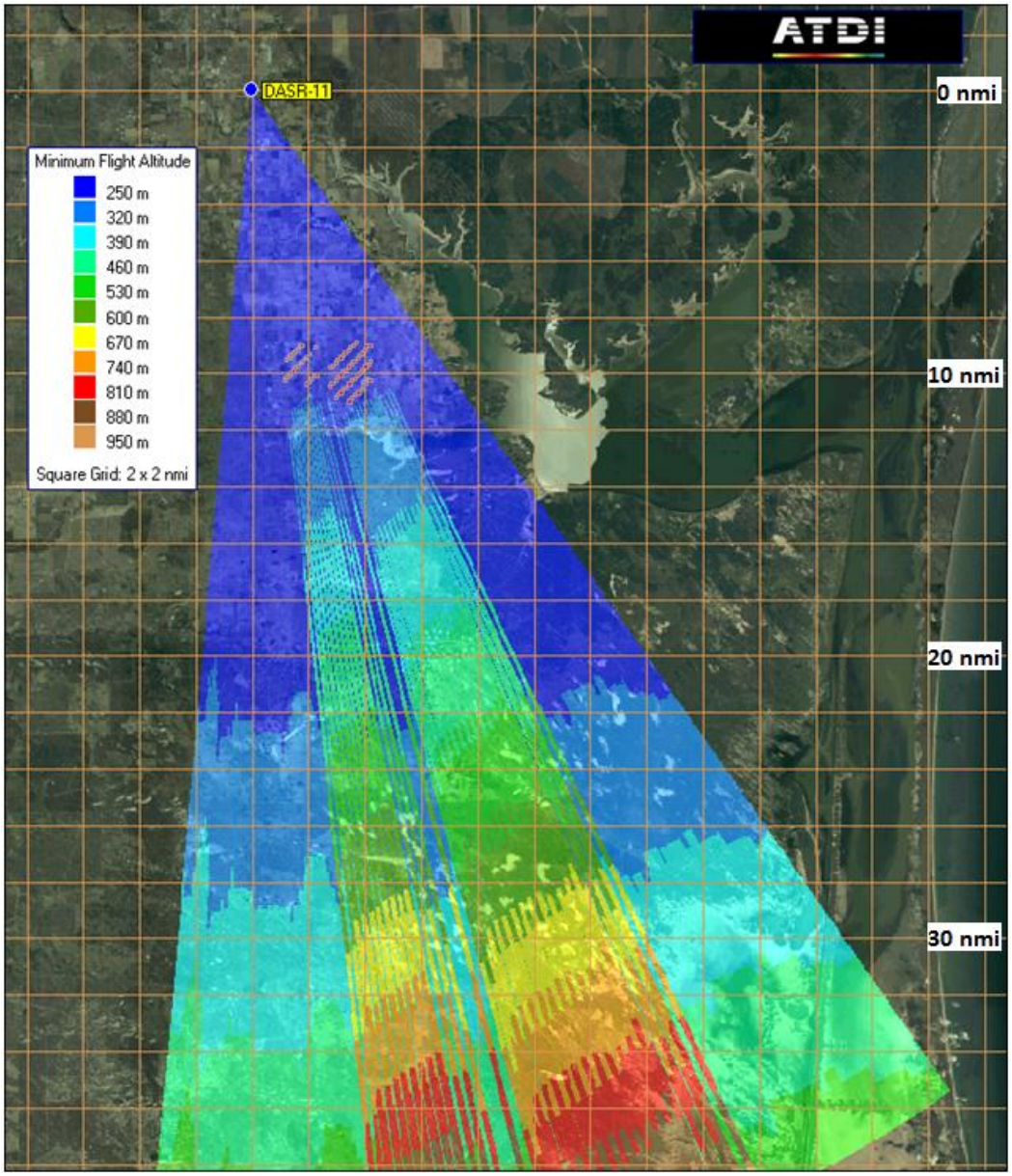

Figure 7: Shadows caused by wind turbines and terrain

5. Wind Turbine Reflection Effect Analysis

Degradation of ATC radar performance occurs when unwanted objects are located within line-of-sight of the radar installation. The degradation applies not only to the shadows that the objects cast, but also applies to the manner in which they scatter the electromagnetic energy that is incident upon them. The unwanted objects can be anomalous terrain, vegetation, buildings, and in this case, wind turbines. The electromagnetic energy transmitted by the radar is incident upon such objects and is potentially reflected back to the radar's receiver, causing clutter returns. The amount of energy that may be reflected back to radar is directly correlated to the radar cross section of the object that the signal is incident upon.

5.1 Wind turbine radio cross section

The radar cross section (RCS) of an object is a measure of how 'large' that object appears to a radar. That is, the RCS shows how detectable the object is when it is within the range of radar. Thus, RCS is directly linked to the maximum detection range for an object. It is affected by many factors, mostly based on the size, shape, and material composition of the object under scrutiny, and the angle of incidence and electromagnetic characteristics of incoming radar signals.

The RCS of a wind turbine, though, is not only dependent on the parameters just stated, but also the direction of the wind, the position of the blades at the time of illumination, the velocity of blade rotation, and many other variable parameters [9]. Changes in wind direction rotate the nacelle and blade rotational axis, altering the turbine's RCS. During each illumination by the radar's main beam, the turbine's blades are at a different orientation. Because of these varying factors and short of complex CAD modeling and hours of RCS prediction processing on high-performance computers, a universal method for determining the exact RCS of a specific turbine located in a specific environment does not exist.

To arrive at a nominal measure of RCS for the Vestas wind turbines to be used at Riviera wind farm and to see if the value falls within the range presented in literature on the subject, the RCS prediction method outlined by the UK's Civil Aviation Authority [10] is used. The methodology is based on the simple scaling of generic RCS values for both the non-moving (tower) and moving (blades) parts of the wind turbine. The table below lists the known and unknown values for this process.

Table 1: Values for RCS calculation

	Generic Wind Turbine	Vestas V90-1.8MV
Tower height	50m	80m
Tower RCS	$80m^2$	?
Blade length	30m	45m
Blade RCS	$9m^2$	?

Scaling factors are derived for the tower and blades separately:

$$A_T = \frac{H_V}{H_G} = \frac{80\ m}{50\ m} = 1.6$$
$$A_B = \frac{L_V}{L_G} = \frac{45\ m}{30\ m} = 1.5 \qquad (3)$$

where

A_T is the tower height scaling factor
H_V is the height of the Vestas turbine
H_G is the height of the generic turbine
A_B is the blade length scaling factor
L_V is the length of the blades of the Vestas turbine
L_G is the length of the blades of the generic turbine

The generic wind turbine RCS values given in the report are then multiplied by these scaling factors to arrive at nominal RCS values for the Vestas V90-1.8MW turbine:

$$RCS_{TV} = RCS_{TG} * A_T = 80\ m^2 * 1.6 = \mathbf{128\ m^2}$$
$$RCS_{BV} = RCS_{BG} * A_B = 9\ m^2 * 1.5 = \mathbf{13.5\ m^2} \qquad (4)$$

where

RCS_{TV} is the RCS of the tower of the Vestas turbine
RCS_{TG} is the RCS of the tower of the generic turbine
RCS_{BV} is the RCS of the blades of the Vestas turbine
RCS_{BG} is the RCS of the blades of the generic turbine

Summing the RCS_{TV} and RCS_{BV} values together, we arrive at a total RCS of 141.5 m^2. When converted to dBsm, the value is:

$$RCS_V = 10\log(141.5) = \mathbf{21.51\ dBsm} \qquad (5)$$

This value is supported by publically accessible documents. Complex computer-aided modeling and use of highly-specialized measurement techniques have yielded time-averaged RCS values between 15 and 20 dBsm by the teams of [9] and [11], who performed the analysis on older, smaller wind turbines. The author of [9] goes on to state that spikes above 30 dBsm are very rare and thus cannot be used reasonably for the safeguarding of radar. Based on the uncertainty of the factors involved in the RCS calculation and the suggestions found in pertinent literature, the value of 30 dBsm may be assumed to provide a conservative estimate of a typical RCS value. In practice, though, it is unlikely that this value will be observed on a regular basis, with the calculated RCS of 21.51 dBsm being more

likely. The 30 dBsm value is used in the calculations and simulations within this report for worst case scenario purposes.

[Interestingly, this range of RCS values is highly relatable to air traffic. While smaller jet fighter aircraft may have RCS values of as little as 0 dBsm (1 m^2) , large aircraft can register at up to and beyond 30 dBsm (1000 m^2), depending on the angle of illumination.]

5.2 Reflection due to wind turbine

Radar signals transmitted by the ATC radar may illuminate all parts of the wind turbine; tower, blades, cone, and nacelle. While the tower and nacelle are stationary (though the nacelle does rotate to a certain degree as wind direction changes), the blades and cone are moving parts. Modern ATC radars are designed to process for and eliminate stationary obstructions, whether they be anomalous terrain of greater altitude, vegetation, or buildings. Based on processing algorithms, these stationary objects are filtered by the radar and do not show up as targets on its user display. Wind turbines, though, create a unique challenge because they are composed of both stationary and rotating parts. With blades that are tens of meters long rotating at speeds determined by the strength of winds, the tips of the blades are likely to be moving at up to 70 meters per second (approximately 160 mph). Such a velocity is nearly identical to the approach, landing, and take-off speeds for airplanes and causes echoes described by the Doppler effect.

Both the stationary portions and moving portions of a wind turbine reflect the previously transmitted electromagnetic waves back into the ATC radar's receiver. Due to the large dynamic range of air traffic control radars and the ability of wind turbines to reflect large amounts of electromagnetic energy back into the receiver, the receiver may become saturated to the point of complete loss of functionality, though this is not likely [12].

As stated in [12], modern radar systems attempt to compensate for the adverse effects created by turbines with complex processing techniques. The Constant False Alarm Rate (CFAR) type of processing technique adjusts a receiver's threshold dynamically to prevent the creation of an excess amount of false alarms due to clutter returns. The algorithm usually functions by subdividing the monitored area into smaller sectors, each with a threshold determined by the amount of clutter in that sector. The clutter returns from a sector containing wind turbines may artificially raise the threshold to a point that the radar may miss target aircraft in that sector.

Modern radar systems employ another processing technique that may partially mitigate the raised thresholds of the CFAR processing techniques. The Moving Target Indication (MTI) and Moving Target Detection (MTD) processing techniques filter incoming electromagnetic energy for frequency shifts caused by moving targets. As mentioned earlier, these frequency shifts are known as the Doppler effect. The quicker an object moves, the greater the Doppler shift it creates. For stationary targets, this is an ideal candidate technique to filter out clutter returns, as reflected energy with small Doppler

shifts may be suppressed completely. Though this works for the turbine tower, the blade tips do rotate at up to 160 miles per hour and thus impart sizable Doppler shifts on the energy they reflect back to the receiver. This yields the possibility of interpreting the moving blades as target aircraft.

Ultimately, the effects of the clutter return on the performance of the radar is based upon the radar's processing techniques, the mitigation techniques employed, the configurability of the system, and the specific conditions created by the presence of a wind farm. A mathematical study of the clutter return is now undertaken for both the primary surveillance radar (PSR).

5.3 PSR antenna patterns

A radar antenna is not an isotropic radiator; it has a highly directional main beam and both horizontal and vertical patterns vary greatly based on angle. For the most thorough and accurate analysis, both the horizontal and elevation (vertical) antenna patterns must be known since variations in gain make a significant impact on power returns to the radar's receiver.

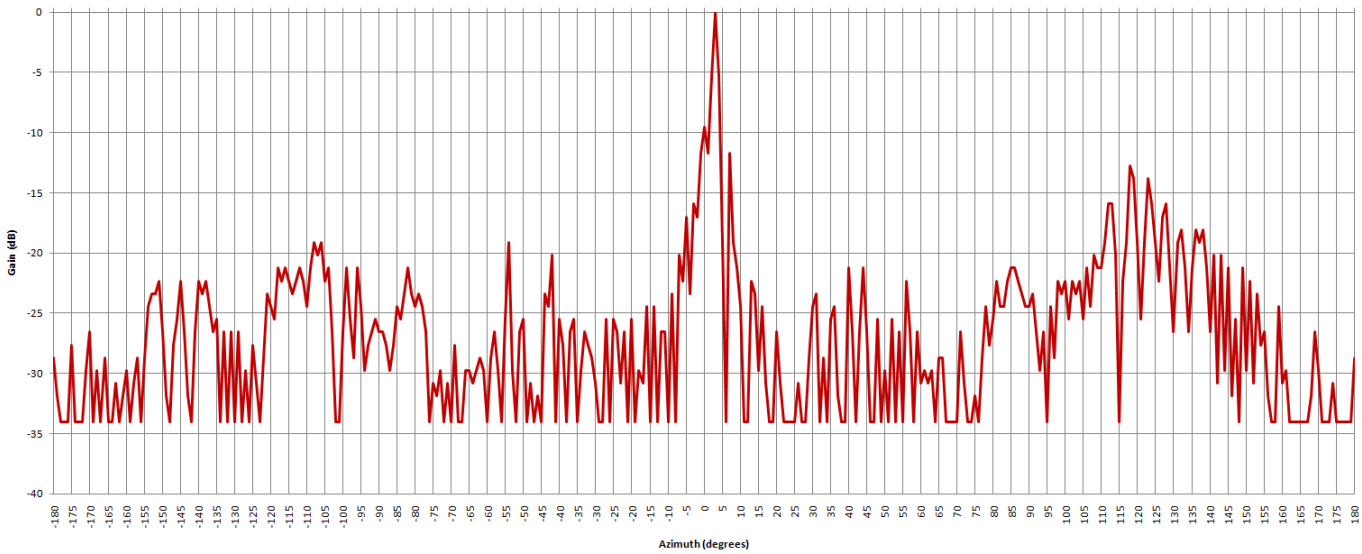

Figure 8: Kingsville DASR-11 Horizontal Antenna Pattern

The horizontal antenna gain pattern above shows a main beam peak of 34 dBi located near the center of the pattern with two prominent side lobes located approximately 120 degrees to either side of the main beam. While the main beam has a peak of 34dBi, the primary side lobes peak at approximately 15 dBi and 20 dBi, respectively. For much of its horizontal rotation, though, the gain for the antenna is between 0 and 15 dBi.

The vertical antenna pattern of the Kingsville DASR-11 is somewhat simpler than its horizontal pattern with fewer peaks and valleys; it is directly influenced by the overall tilt of the antenna. The available

tilt range is between 3° below parallel to horizontal to 5° above parallel to horizontal. The typical vertical antenna pattern (obtained from Raytheon's ASR-11 product description document) may be seen in the figure below.

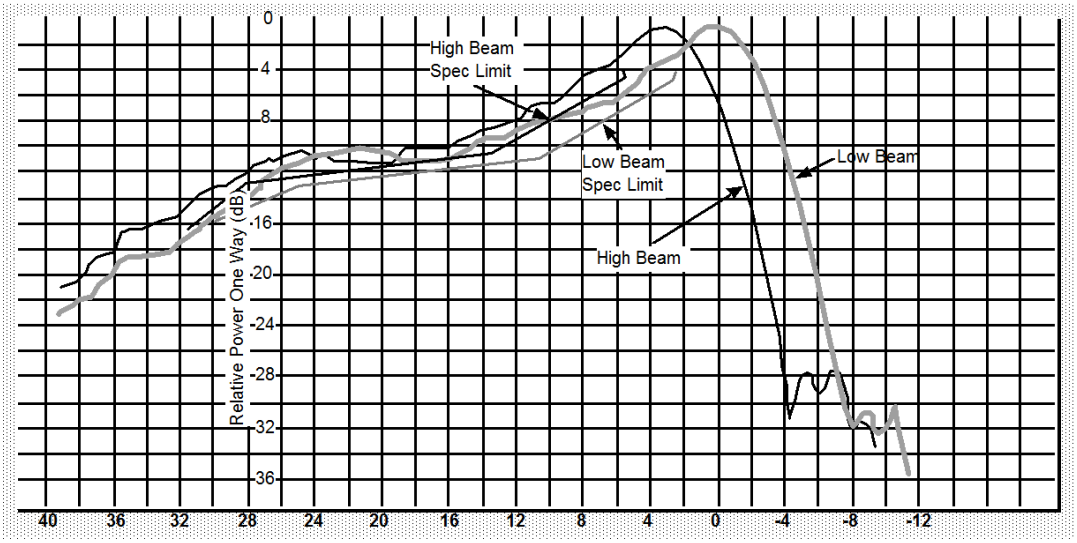

Figure 9: Typical PSR Antenna Elevation Pattern Characteristics

The DASR-11 installed at Naval Air Station Kingsville has a 3 degree tilt above parallel with horizontal. Due to the large distance between the radar and the wind turbines and the height of the wind turbines (which is minute relative to the distance between the radar and the turbines), the angle subtended by a wind turbine in the radar's elevation pattern is less than 0.3°. Because of this small angle, it is possible to associate one overall directivity loss for the low beam and one overall directivity loss for the high beam. As shown in the figure below, adjusted for the 3 degree tilt above parallel with horizontal, the low beam has an overall loss of 5.5 dB while the high beam has an overall loss of 20 dB.

The radar system is capable of scanning the skies for airborne targets using two different antenna patterns. The low beam is used to scan for targets that are further away and thus at a lesser elevation angle with respect to the antenna. The pattern is thus tailored to offer greater directivity at lesser elevation angles. As targets approach the radar, they begin encroaching upon regions of the low beam antenna pattern that do not offer as much gain, and are thus less likely to be detected. To avoid potential target loss, the radar system is able to switch to a high beam pattern, which offers more gain at greater elevation angles with respect to the radar. The DASR-11 ATC is able to switch between the two antenna patterns continuously.

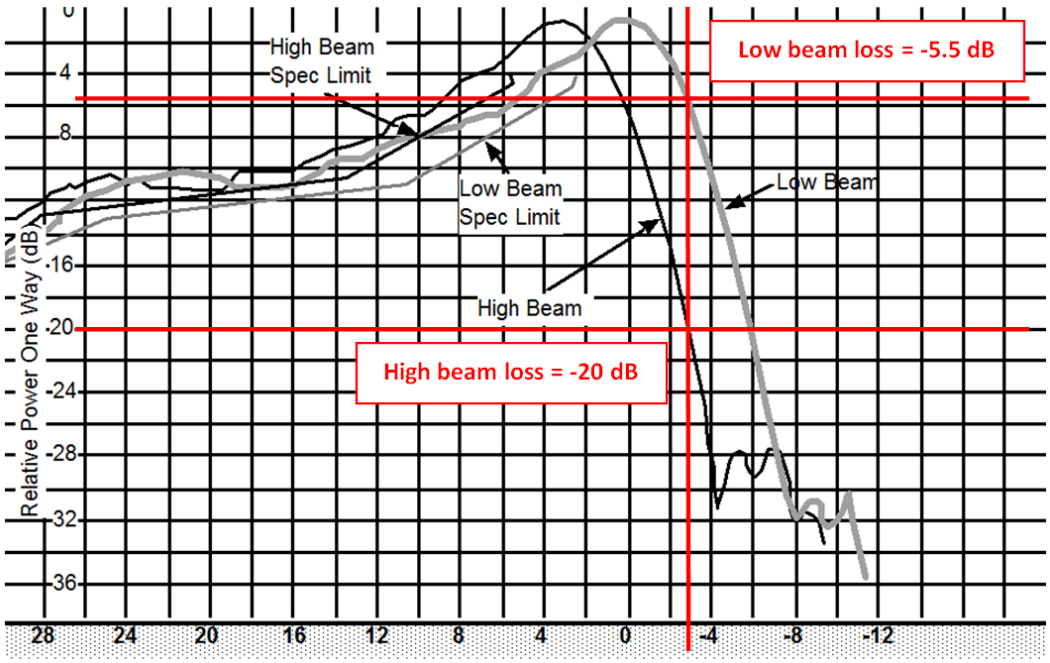

Figure 10: Effects of radar antenna tilt on elevation radiation pattern

5.4 PSR clutter return at 2785MHz operating frequency – low beam

As explored in NTIA Technical Report TR-08-454, a modified version of the radar equation may be used to calculate clutter returns to the radar installation. The methodology followed in that report is implemented here. The radar equation is as follows:

$$P_{rx} = \frac{P_{tx} * g_{tx} * g_{rx} * \sigma * \lambda^2}{64 * \pi^3 * d^4} \qquad (6)$$

where

P_{rx} is received clutter return power in Watts
P_{tx} is transmitted power in Watts
g_{tx} is the gain of the transmitter antenna
g_{rx} is the gain of the receiver antenna
σ is the RCS of the wind turbine in m^2
λ is wavelength in meters
d is distance between radar and wind turbine in meters

The specifications of the ASR-11 PSR emission are given in the table below, originally from SFAF (Standard Frequency Action Format) record provided by Naval Air – Kingsville, TX. The line numbers

and values are obtained from the report while the parameter and meaning fields are obtained by comparison with the MCEB Pub 7 document:

Table 2: ASR-11 PSR specifications

Line No.	Parameter	Value	Meaning
110	Frequency	M2785	2785 MHz
114	Emission Designator	2M80Q3N	2.8 MHz
115	Transmit Power	K25	25 kW
116	Power Type	P	Peak envelope power
117	Effective Radiated Power	108	108 dBm
300	State/Country	TX	Texas
301	Antenna Location	KINGSVILLE	Kingsville
303	Antenna Coordinates	273035N0974812W	WGS 84 datum latitude & longitude
356	Antenna Structure Height	17	17 m above ground level
357	Transmit antenna Gain	34	34 dBi
358	Antenna Elevation	6	6 m above sea level
457	Receive Antenna Gain	34	34 dBi

Because the ASR-11 is an air traffic control radar, its transmitter antenna and receiver antenna gains are the same. The gain values are in terms of dBi; that is, with regards to an isotropic radiator:

$$g_{tx} = g_{rx} = 34\ dBi = 2511.886 \qquad (7)$$

The main lobe of the radar, at the peak of the radar's directivity, has a gain factor of 2511.886 to 1. The gain factor for the side lobes of the horizontal pattern is much lesser, with the primary side lobes offset by ±120 degrees from the main lobe having a gain factor of approximately 125 to 1, or 20 dBi. The characteristics of the antenna elevation pattern must also be accounted for. For the low beam, there is a loss of 5.5 dB produced by the 3 degree tilt of the antenna. That yields a lesser gain of:

$$g_{tx} = g_{rx} = 34\ dB - 5.5\ dB = 28.5\ dB = 707.946 \qquad (8)$$

The RCS of the wind turbines, σ, is taken to be the conservative value assumed in the previous section. Given the LOS path profiles shown in Section 4, we can assume that the prevailing majority of each wind turbine is illuminated by the radiation pattern, even with some terrain shadowing. The validity of this assumption is further supported by the fact that the greatest deviations in a wind turbine's RCS are caused by the rotating blades, as seen in [11] and [14], which are at the greatest elevation and therefore most likely to be illuminated. Thus:

$$\sigma = 30\ dBsm = 1000\ m^2 \qquad (9)$$

The ASR-11 radar at the Kingsville location operates at frequencies of 2785 MHz and 2865 MHz. Since the operating frequency is inversely proportional to wavelength and we seek to examine the worst case scenario, the 2785 MHz frequency is selected for consideration because it yields a longer wavelength and thus a greater clutter return power to the receiver. At 2785 MHz, the wavelength is:

$$\lambda = \frac{c}{f} = \frac{3*10^8\ {}^{m}/_{s}}{2785\ MHz} = 0.1077\ m \tag{10}$$

Since each turbine has a unique distance to the radar, the basic radar equation is simplified to be a function of distance. For this equation, we assume that each wind turbine is being illuminated by the main beam of the radar (with both transmitter gain and receiver gain of 34dBi), yielding maximum power return:

$$P_{rx}(d) = \frac{P_{tx} * g_{tx} * g_{rx} * \sigma * \lambda^2}{64 * \pi^3 * d^4} = \frac{25\ kW * 707.946^2 * 1000\ m^2 * (0.1077\ m)^2}{64 * \pi^3 * d^4}\ W$$

$$P_{rx}(d) = \frac{7.324 * 10^7}{d^4}\ W \tag{11}$$

In logarithmic notation, and assuming $g_{tx} = g_{rx} = g$, that is:

$$P_{rx}(d) = 10\log(P_{tx}) + 20\log(g) + 10\log(\sigma) + 20\log(\lambda) - 10\log(64\pi^3) - 40\log(d)\ dBW$$

$$P_{rx}(d) = 78.647 - 40\log(d)\ dBW = 108.719 - 40\log(d)\ dBm \tag{12}$$

The distance between the radar and the turbines varies from just under 17 kilometers (~9 nmi) to over 21 kilometers (~11.5 nmi). Evaluating for the turbines located closest and furthest away and then averaging to arrive at a aeverage value, the values in the table below are obtained.

Table 3: Clutter return to PSR at 2785 MHz – low beam

	Turbine No.	Distance to PSR (m)	Distance to PSR (nmi)	Clutter return (W)	Clutter return (dBm)
Closest to PSR	8	16939 m	9.146 nmi	$8.896*10^{-10}$ W	-60.51 dBm
Furthest from PSR	68	21295 m	11.498 nmi	$3.561*10^{-10}$ W	-64.48 dBm
Average	N/A	19031 m	10.276 nmi	$5.772*10^{-10}$ W	-62.39 dBm

According to NTIA Technical Report TR-08-454, the output power of the radar is to be further multiplied by its pulse compression ratio (PCR). That ratio is 89:1 and would yield greater interference if applied with an average clutter return of -43.04 dBm. For this study, the method is not applied.

A simulation is performed in HTZ Warfare using the Windfarm Turbine Interference report function, as shown in the figure below.

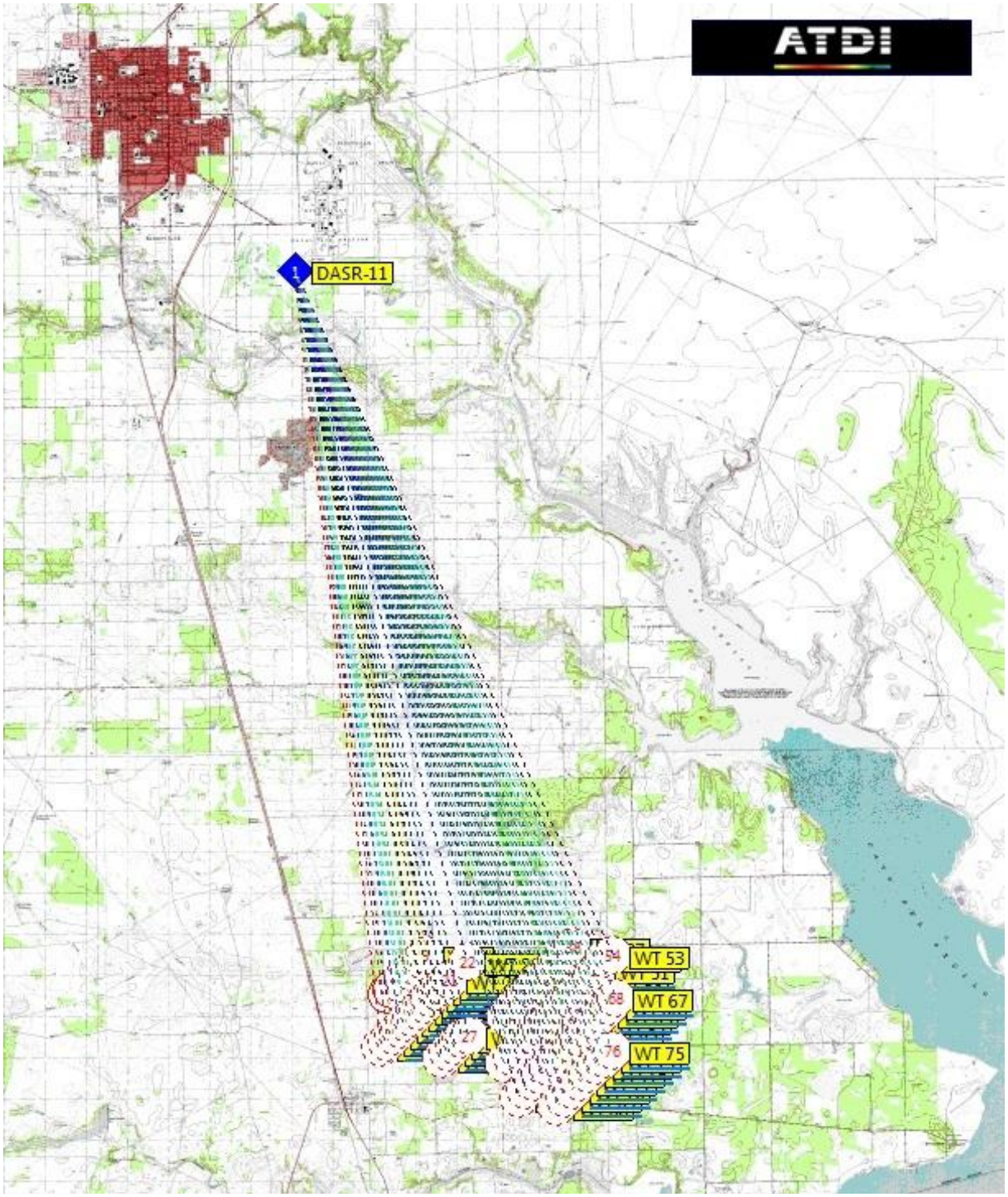

Figure 11: PSR windfarm clutter return simulation in HTZ Warfare

The simulation yielded very similar results to the mathematical approach undertaken previously. The table below compares the values obtained through both the mathematical calculation and the HTZ Warfare simulation, with the full list of clutter returns caused by individual turbines in Appendix A.

Table 4: Comparison of clutter returns from mathematical model and HTZ Warfare simulation – low beam

	Turbine No.	Distance to PSR (m)	Distance to PSR (nmi)	Clutter return-mathematical model	Clutter return-HTZ Warfare simulation
Closest to PSR	8	16939 m	9.146 nmi	-60.51 dBm	-60.51 dBm
Furthest from PSR	68	21295 m	11.498 nmi	-64.48 dBm	-64.48 dBm
Average	N/A	19031 m	10.276 nmi	-62.39 dBm	-62.39 dBm

The radar receiver's sensitivity must be calculated to have a term to compare the clutter return values to. Also known as the noise floor of the receiver, the equation is:

$$Nf\ (dBm) = -174 + 10 * \log(B_{IF}) + NF \qquad (13)$$

where

Nf is the noise floor in dBm
B_{IF} is the IF bandwidth of the radar in Hz
NF is the noise figure in dB

The IF bandwidth of the radar is 2.8 MHz and the noise figure is assumed to be 5 dB for an ATC radar of this type (though noise figure values range from 4 to 12 dB):

$$Nf\ (dBm) = -174 + 10 * \log(2.8 * 10^6) + 5 = -104.528\ dBm \qquad (14)$$

The highest permissible interference-to-noise ratio before radar performance degradation occurs is -9 dB [13]. Using this value and the noise floor for the radar, we arrive at a performance threshold:

$$P_{threshold} = Nf\ (dBm) - 9\ dB = \mathbf{-113.528\ dBm} \qquad (15)$$

With an average clutter return of -62.39 dBm, the energy scattered from the wind turbines greatly surpasses the radar's performance threshold, which may lead to target loss. This is only the case, though, when a wind turbine is illuminated by the radar's main beam, at peak gain. However, with such a high peak clutter return value that so greatly surpasses the performance threshold of the radar, it is necessary to perform an analysis to see whether or not the clutter returns resultant from side lobe illumination will also yield lost targets. To perform the clutter return versus azimuth analysis, the horizontal antenna pattern of the radar is necessary; it can be seen in the previous section.

Accounting for both the horizontal and vertical antenna patterns and assuming a radar cross section of 30 dBsm for the individual wind turbines, a graph is created to correlate the clutter return from a

single wind turbine to an aircraft target's power return as a function of distance, where both target aircraft and wind turbine are assumed to be at the same distance from the radar. The aircraft is assumed to have a radar cross section of 1 m^2 and its power return is held constant, assuming it is illuminated by the radar's main beam with no loss due to the elevation pattern (thus gain of 34 dBi) throughout the radar antenna's rotation. The clutter return from the wind turbine is a function of the gain associated with the radar's azimuth orientation and the elevation pattern loss of 5.5 dB. The two are plotted for the same distance from the radar. Furthermore, the nominal receiver performance threshold and the increased receiver performance threshold are plotted. The increased receiver performance threshold is a summation of the nominal receiver performance threshold and clutter return power when the clutter return surpasses the nominal threshold value. Effectively, the nominal receiver performance threshold can be seen as N (noise), while the raised receiver performance threshold is I+N (interference plus noise). Plots for distances of 9 nmi and 11.5 nmi (for the nearest and furthest wind turbine, respectively) follow.

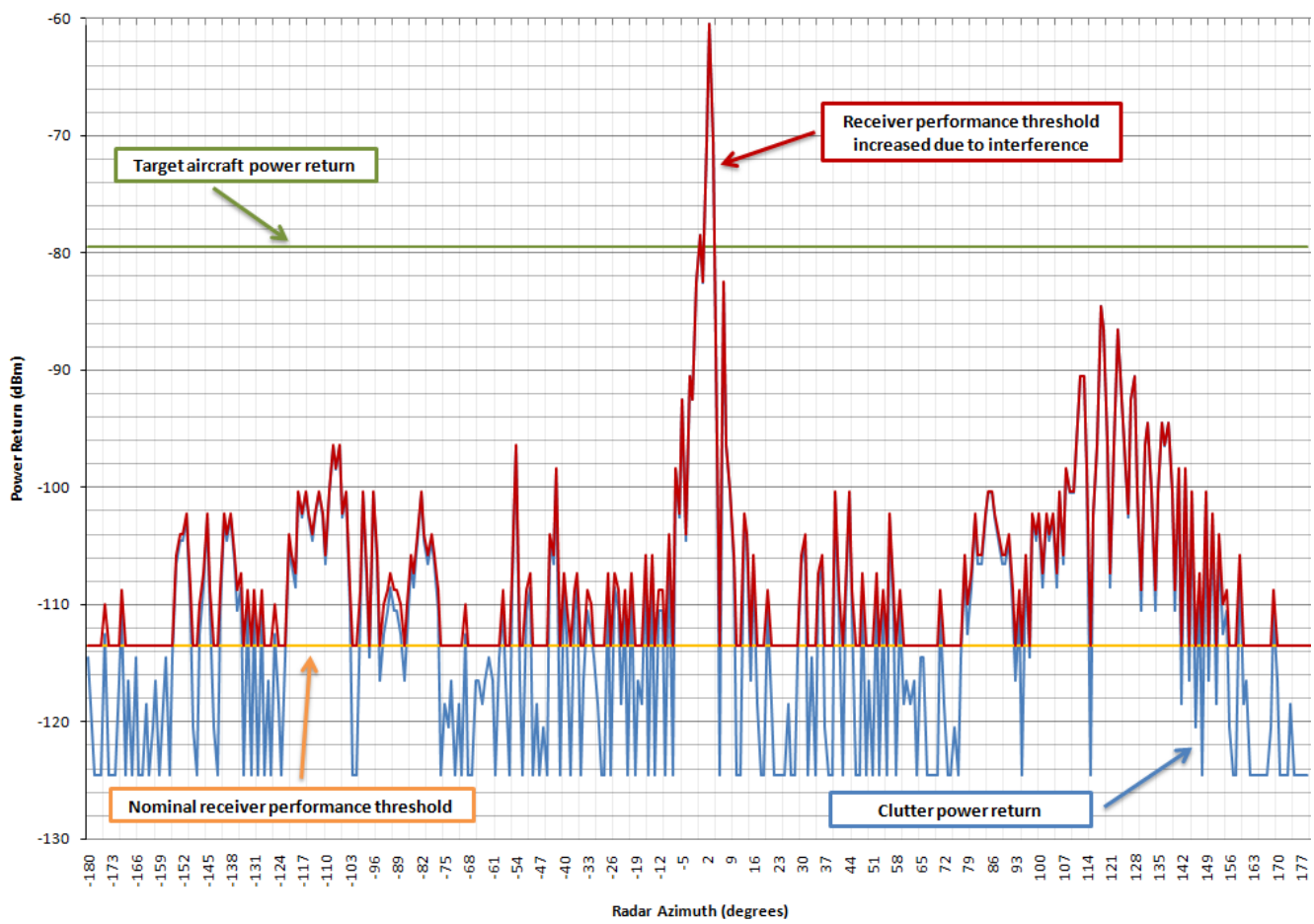

Figure 12: Clutter return from single wind turbine vs. radar azimuth (9 nmi) – low beam

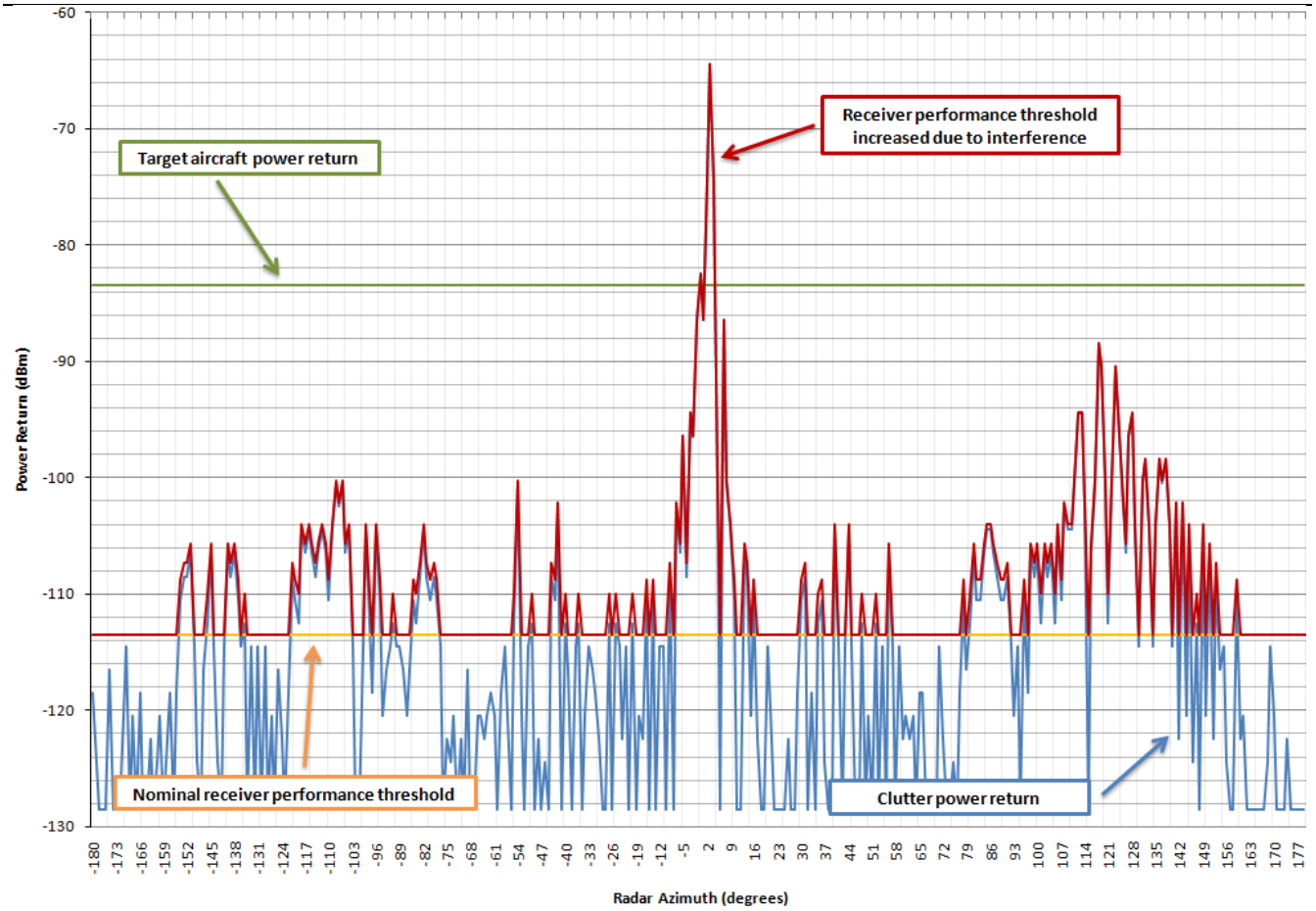

Figure 13: Clutter return from single wind turbine vs. radar azimuth (11.5nmi) – low beam

From the two previous figures it is apparent that the clutter return from a single wind turbine not only exceeds the nominal receiver performance threshold, but that the power return from a target aircraft is surpassed when a wind turbine is illuminated by the main beam. When both the aircraft target and the wind turbine are illuminated by the main beam, the power return from the turbine is 20 dB greater than the power return from the airborne target. Also, the clutter returns from the wind turbine surpass the receiver's nominal performance threshold, increasing it on average by 15 dB and by nearly 50 dB for the main beam. This produces a 7 degree swath in the rotation pattern where the aircraft target is likely not to be detected as the radar is saturated by power returns from the wind turbine. Once an entire wind farm is considered, it is expected that the affected azimuths will grow in size. The entire 75 wind turbine wind farm is considered in Section 6 of this report, as well as the 'twinkling' effect that it may produce.

5.5 PSR clutter return at 2785 MHz operating frequency – high beam

As mentioned earlier, the primary surveillance radar of the ASR-11 air traffic control system uses two beam patterns as it scans the skies for airborne targets. The high beam, used for detection of targets that are closer to the radar installation, has higher gain for greater elevations with respect to the radar antenna. Thus, the gain of the system is lesser for targets that are closer to horizontal, of lesser height above sea level. The same approach used in the low beam analysis is employed here to study the clutter effects upon the radar for the high beam antenna pattern at peak gain. The gain is the only part of the equation that is modified, with a loss of 20 dB incorporated due to the elevation antenna pattern characteristics:

$$g_{tx} = g_{rx} = 34\ dB - 20\ dB = 14\ dB = 25.119 \tag{16}$$

This yields a new gain term for the power return equation:

$$P_{rx}(d) = \frac{P_{tx} * g_{tx} * g_{rx} * \sigma * \lambda^2}{64 * \pi^3 * d^4} = \frac{25\ kW * 25.119^2 * 1000\ m^2 * (0.1077\ m)^2}{64 * \pi^3 * d^4}\ W$$

$$P_{rx}(d) = \frac{9.220 * 10^4}{d^4}\ W \tag{17}$$

In logarithmic notation, and assuming $g_{tx} = g_{rx} = g$, that is:

$$P_{rx}(d) = 10\log(P_{tx}) + 20\log(g) + 10\log(\sigma) + 20\log(\lambda) - 10\log(64\pi^3) - 40\log(d)\ dBW$$

$$P_{rx}(d) = 49.647 - 40\log(d)\ dBW = 79.647 - 40\log(d)\ dBm \tag{18}$$

Evaluating these equations for the nearest, furthest, and average distances between the wind turbines of the Riviera wind farm and the NAS Kingsville radar, the clutter returns for both the mathematical calculation and HTZ Warfare simulation are as listed in the table below:

Table 5: Comparison of clutter returns from mathematical model and HTZ Warfare simulation - high beam

	Turbine No.	Distance to PSR (m)	Distance to PSR (nmi)	Clutter return-mathematical model	Clutter return-HTZ Warfare simulation
Closest to PSR	8	16939 m	9.146 nmi	-89.51 dBm	-89.51 dBm
Furthest from PSR	68	21295 m	11.498 nmi	-93.48 dBm	-93.48 dBm
Average	N/A	19031 m	10.276 nmi	-91.53 dBm	-91.52 dBm

Compared with the returns from the low beam, the returns from the high beam are lower and thus closer to the nominal receiver performance threshold. Assuming an airborne target illuminated by the full power of the high beam with undiminished gain for all azimuths, an analysis is performed to

yield the clutter return from a single wind turbine versus radar azimuth for wind turbines of distances 9 nautical miles and 11.5 nautical miles from the radar. The plots are below.

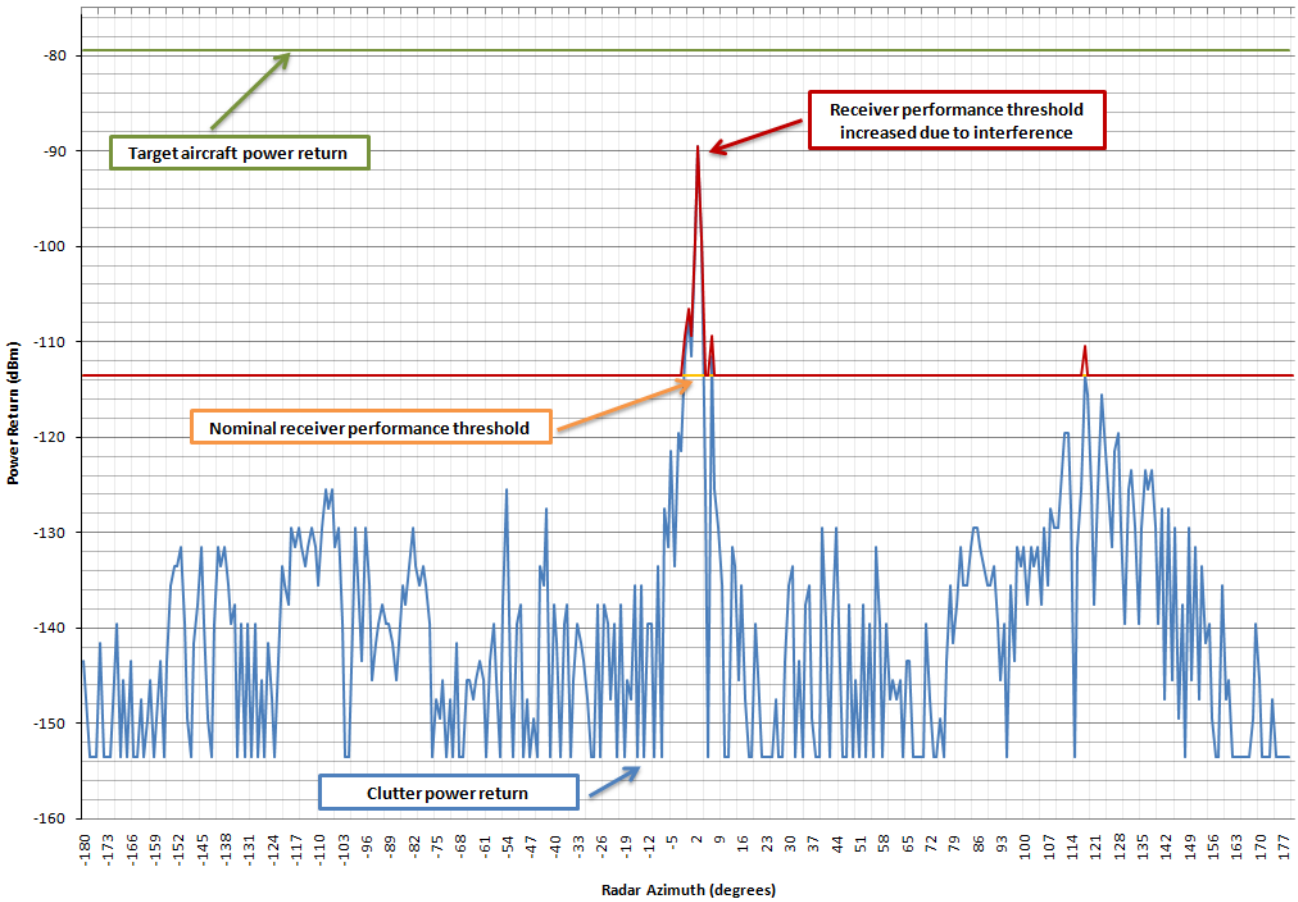

Figure 14: Clutter return from single wind turbine vs. radar azimuth (9 nmi) – high beam

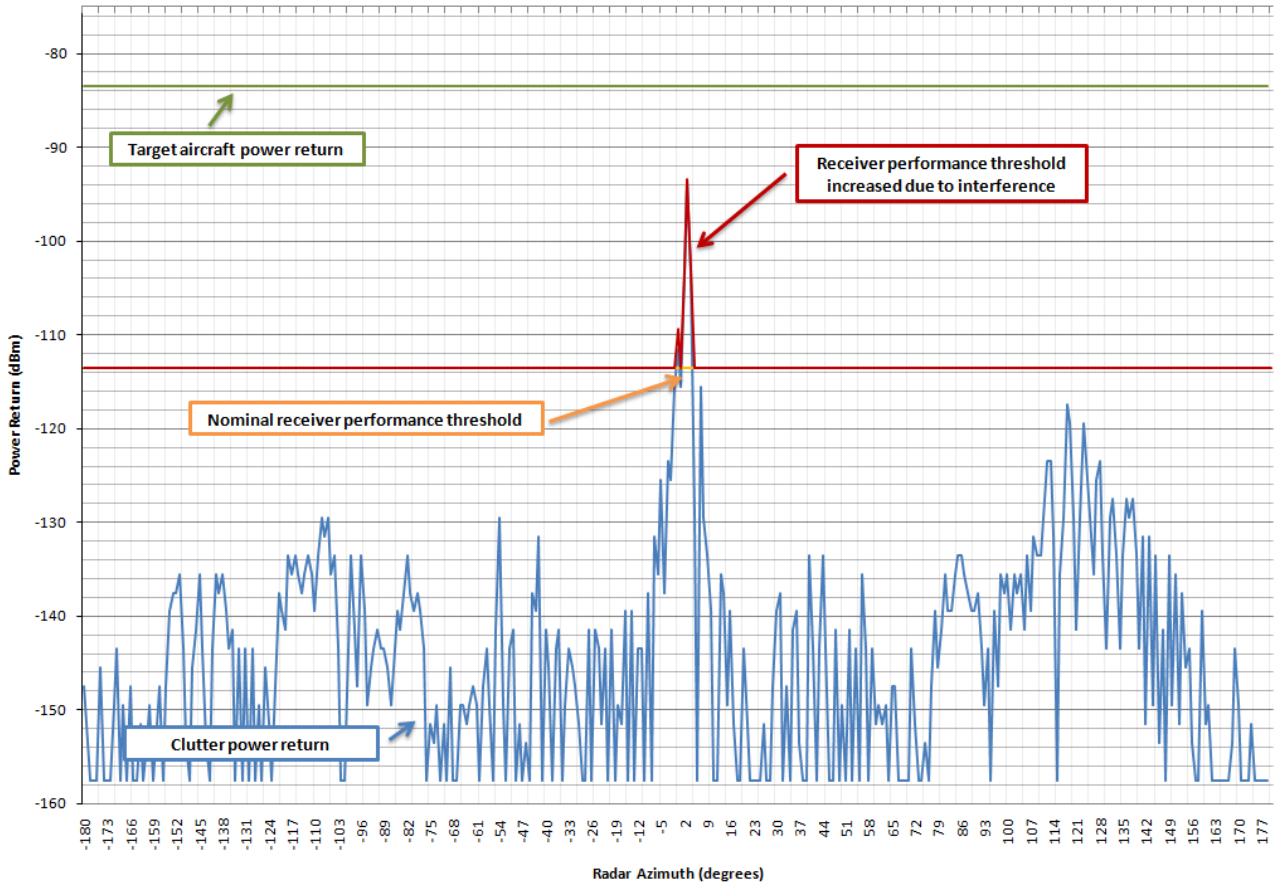

Figure 15: Clutter return from single wind turbine vs. radar azimuth (11.5 nmi) – high beam

Unlike the results for the PSR low beam, the clutter return from a single wind turbine surpasses the nominal receiver performance threshold only when the main beam is pointing directly at the wind turbine. This leads to a single spike in the increased receiver performance threshold due to interference. The target aircraft power return (when both the aircraft and the wind turbine are at the same distance from the radar antenna) is not surpassed at any point. This means that a single wind turbine in the line-of-sight of the high beam of the radar should not produce target loss at any azimuth. The overall effects of an entire wind farm on the high beam are analyzed in Section 6.

6. Aggregated Wind Turbine Effects

Given the impact of a single wind turbine on the receiver performance threshold, it is logical that a wind farm of 75 turbines will have a greater overall effect upon the functional performance of the ASR-11 radar at Kingsville NAS. It is important to note that the individual turbines of the farm are not located at a single azimuth with respect to the radar. They are spread over an azimuth of 19°, as the figure below portrays, with turbines between 9 nautical miles and 11.5 nautical miles from the radar.

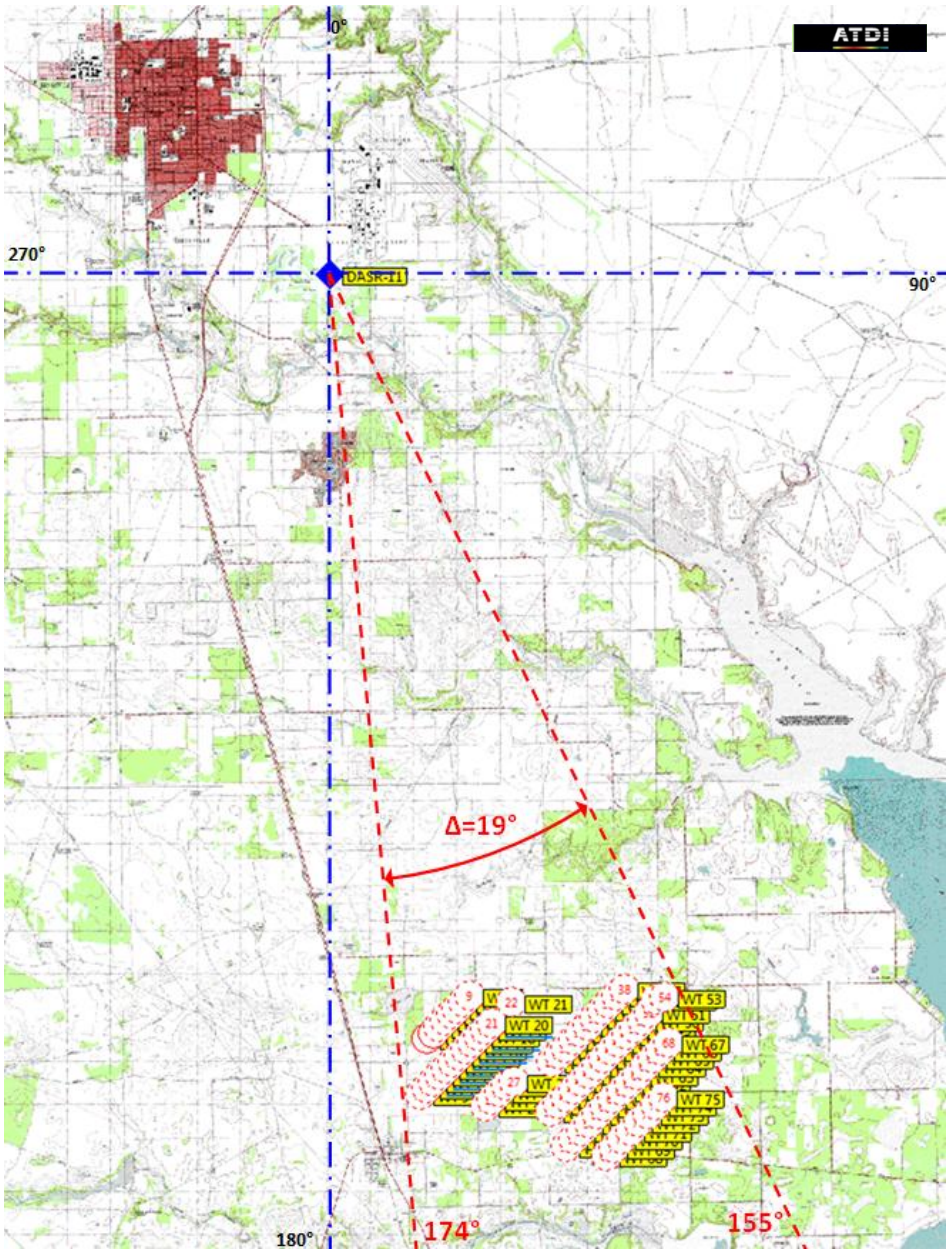

Figure 16: Proposed location of wind farm and its azimuth with respect to the ASR-11 radar

6.1 Number of wind turbines per resolution cell

The PSR in use at NAS Kingsville has a range resolution of 0.125 nmi at 0.8 Pd (probability of detection) and an azimuth resolution of less than 2.6° at 0.8 Pd. Since the exact parameters for the resolution cells in use at NAS Kingsville are unknown, these two specifications from the DASR-11 product data sheet are used to establish the resolution cells centered about the radar. For computational simplicity, the azimuth resolution used is 2.5° per cell with cells 0.125 nmi in radial height. The below figure shows how the wind turbines may potentially fall into the resolution cells created by these two dimensions.

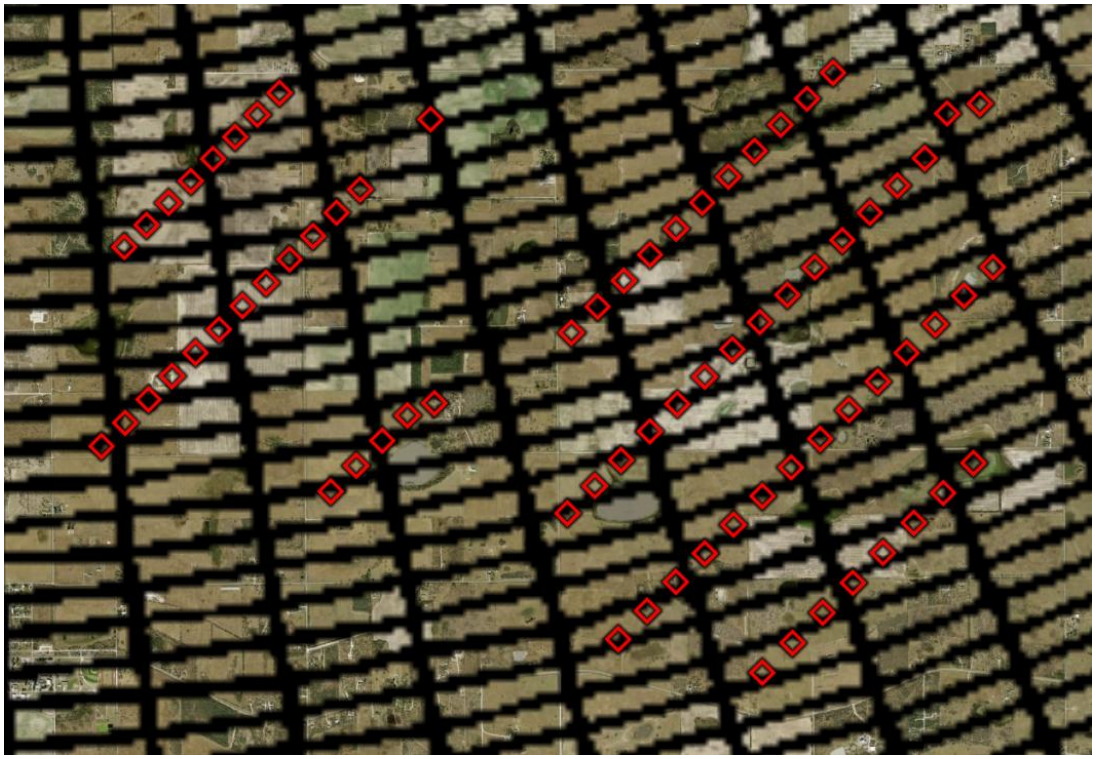

Figure 17: Wind turbines within resolution cells

From the above figure, it is apparent that no more than three wind turbines may potentially fall within a single resolution cell. When one wind turbine falls within a resolution cell, the maximum and minimum clutter return plots in Sections 5.4 and 5.5 for clutter returns for the low beam and high beam result. If two turbines fall within a resolution cell, the clutter return to the radar is raised by 3 dB over that of a single turbine. If three turbines fall within a resolution cell, the clutter return to the radar is raised by 6 dB over that of a single turbine. The increases in clutter return from more than one turbine in a resolution cell do not alter the overall performance of the radar. For the low beam, given these and previous assumptions, the increase in clutter return from a cell will only raise the already increased receiver performance threshold. A target aircraft will still be detected at all azimuths other than those occupied by both a wind turbine and the target aircraft at the same time.

For the high beam, there should be no qualitative change in performance either. The nominal receiver performance threshold should continue to be breached only for the main beam of the radar and there should still be little chance of target loss.

6.2 Resolution cells with likely target loss

Due to the angular width of the radar's main beam, target loss is not only possible in a cell occupied by a wind turbine, but also in cells adjacent in azimuth and possibly in range as well. Here, we only consider cells neighboring in azimuth due to the thickness of the radar's main beam. The image below shows the resolution cells occupied by wind turbines in red. Cells in orange are adjacent cells where target loss is also possible.

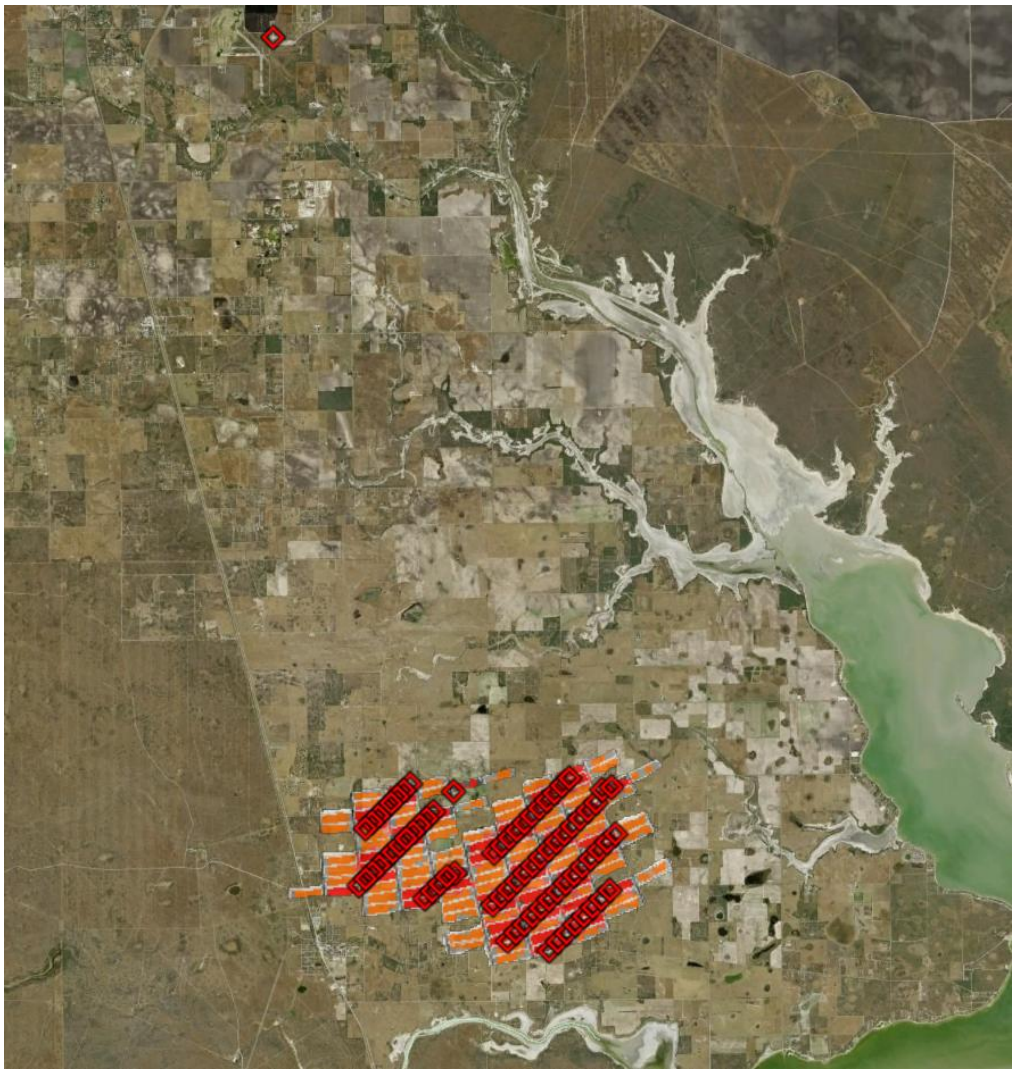

Figure 18: Resolution cells with possible target loss

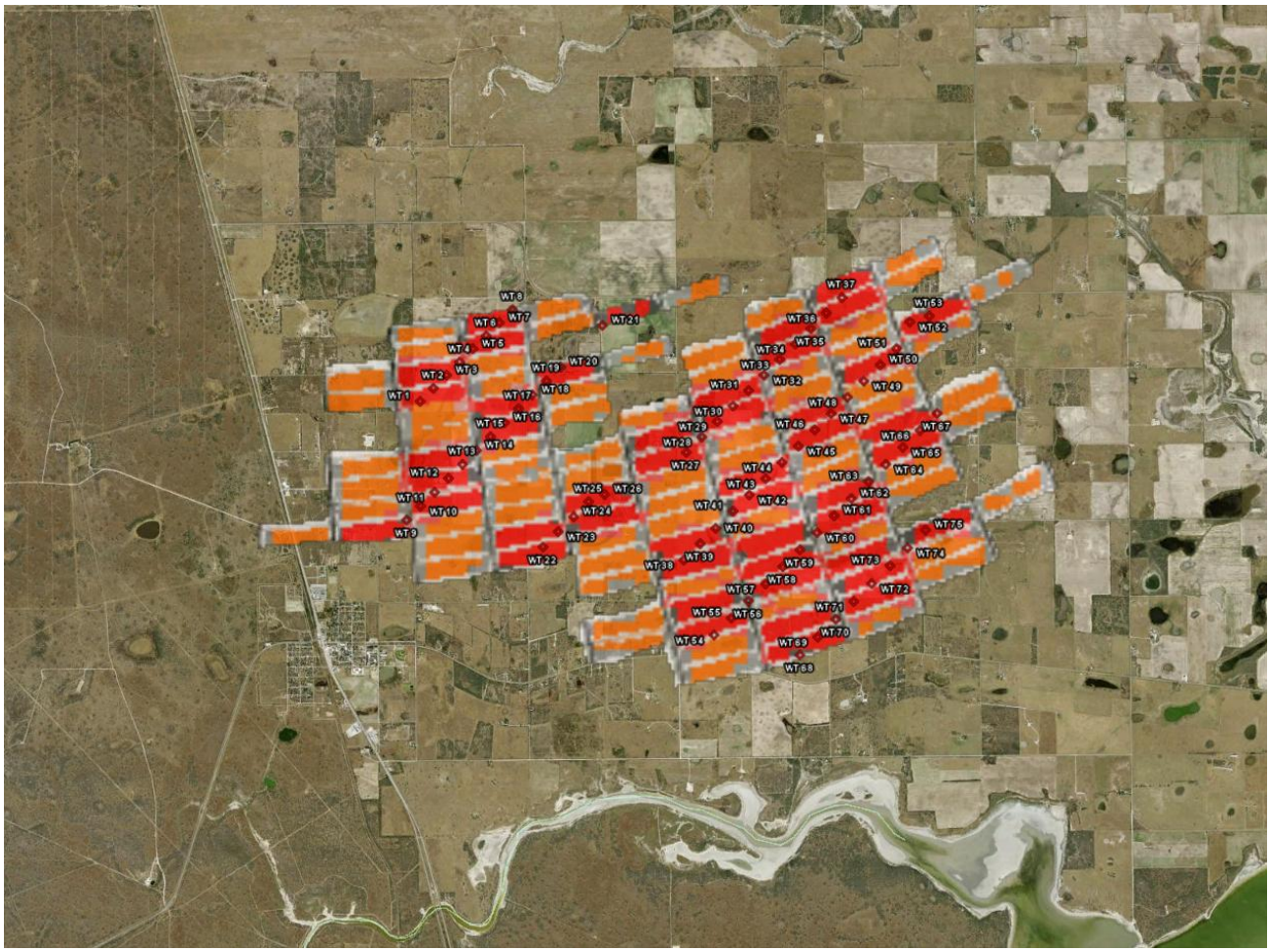

Figure 19: Detail of resolution cells with possible target loss

Assuming the use of the nominal resolution cell sizes of 2.5° in azimuth and 0.125 nmi in range, 47 resolution cells contain at least one wind turbine (red in the above images). A further 67 resolution cells may still contain strong enough clutter return yielding target loss due to the width of the main beam (those cells are orange). For the area within a 12 nautical mile radius of the PSR, 0.34% cells will potentially yield clutter returns higher than aircraft target returns due to turbines within the cell. A further 0.48% of resolution cells will potentially yield target loss due to their azimuth proximity to cells containing wind turbines. In total, 114 resolution cells may be affected, accounting for 0.82% of the cells located within a 12 nautical mile radius of the radar. With regards to area, approximately 2.6 nmi^2 of the 452 nmi^2 within the 12 nautical mile radius of the radar are directly affected by turbines, while a further 3.8 nmi^2 represent areas where target loss is possible due to proximity to cells containing wind turbines. The total affected area is thus 6.4 nmi^2. With regards to percentage of area within a 12 nautical mile radius of the radar, that is 0.58% area for turbines in resolution cells, 0.84% area for neighboring cells, and 1.42% overall.

For the detection radius of 60 nautical miles, the cells where target loss is possible represent 0.07% of resolution cells. Cells that are potentially effected due to their azimuth proximity to the cells containing turbines add another 0.1% for a total of 0.17% cells effected within a radius of 60 nautical miles of the radar installation. The total effected area comes out to be approximately 0.057% of the overall area swept by a 60 nmi radius radar. Target loss is possible for both the low beam and the high beam, though the low beam has a greater chance of being effected due to higher gain at lower altitudes.

6.3 False targets caused by the 'twinkling' effect

As described in [15] and [16], PSR radar may experience the 'twinkling' effect caused by a wind farm. This effect is the result of the varying blade rotational speeds and angles of illumination caused by changing wind conditions. While a given turbine's blades may be fully illuminated during one radar sweep, its neighbor's may be fully illuminated during the next sweep. This causes confusion for the radar, interpreting the two returns as a moving target due to the similar Doppler shift to the frequency of the returned energy and the geographical displacement from one turbine to the next. In this way, a row of wind turbines illuminated during consecutive radar sweeps may potentially create a false target. Due to the planned orientation of the wind turbines at Riviera wind farm, the generation of false targets is more likely as the turbines are arranged in rows with turbines illuminated serially in each row as the radar sweeps from one end to the other. Since this effect is random and its duration is brief, the turbines appear to 'twinkle' on the radar display.

Due to the strength of the clutter returns from the wind turbines and their quantity in close proximity to each other, false targets are not only possible in the resolution cells where the turbines are located, but also at azimuths where the radar's side lobe gain is high enough to make the turbine return power surpass the nominal receiver performance threshold. In essence, false target plots may appear anywhere within a ring of minimum radius corresponding to the distance from the radar to the nearest turbine and a maximum radius corresponding to the distance from the radar to the furthest turbine. Thus, this ring stretches from approximately 9 nautical miles from the radar to 11.5 nautical miles from the radar. Within this ring are encompassed 2736 resolution cells, assuming the nominal resolution cell size of 2.5° in azimuth and 0.125 nautical miles in range. Assuming a 60 nmi detection range with cells of the nominal size (for a total of 54,720 resolution cells), 5% of the total number of cells see potential for false target plots and thus the twinkling effect. The area potentially affected by the twinkling effect is 154 nmi^2, representing 1.4% of the 11,310 nmi^2 covered by the PSR.

The following two images show this ring situated around the NAS Kingsville PSR. The first image portrays the overall ring as a constellation of concentric rings caused by individual turbines of the proposed wind farm. The denser the concentration of rings, the more likely a false target is to be generated. The second image portrays the potential false target zone as a yellow ring (the turbines are represented as red symbols upon the ring) and adds a 60 nautical mile radius circle that shows the extent of the PSR's detection range.

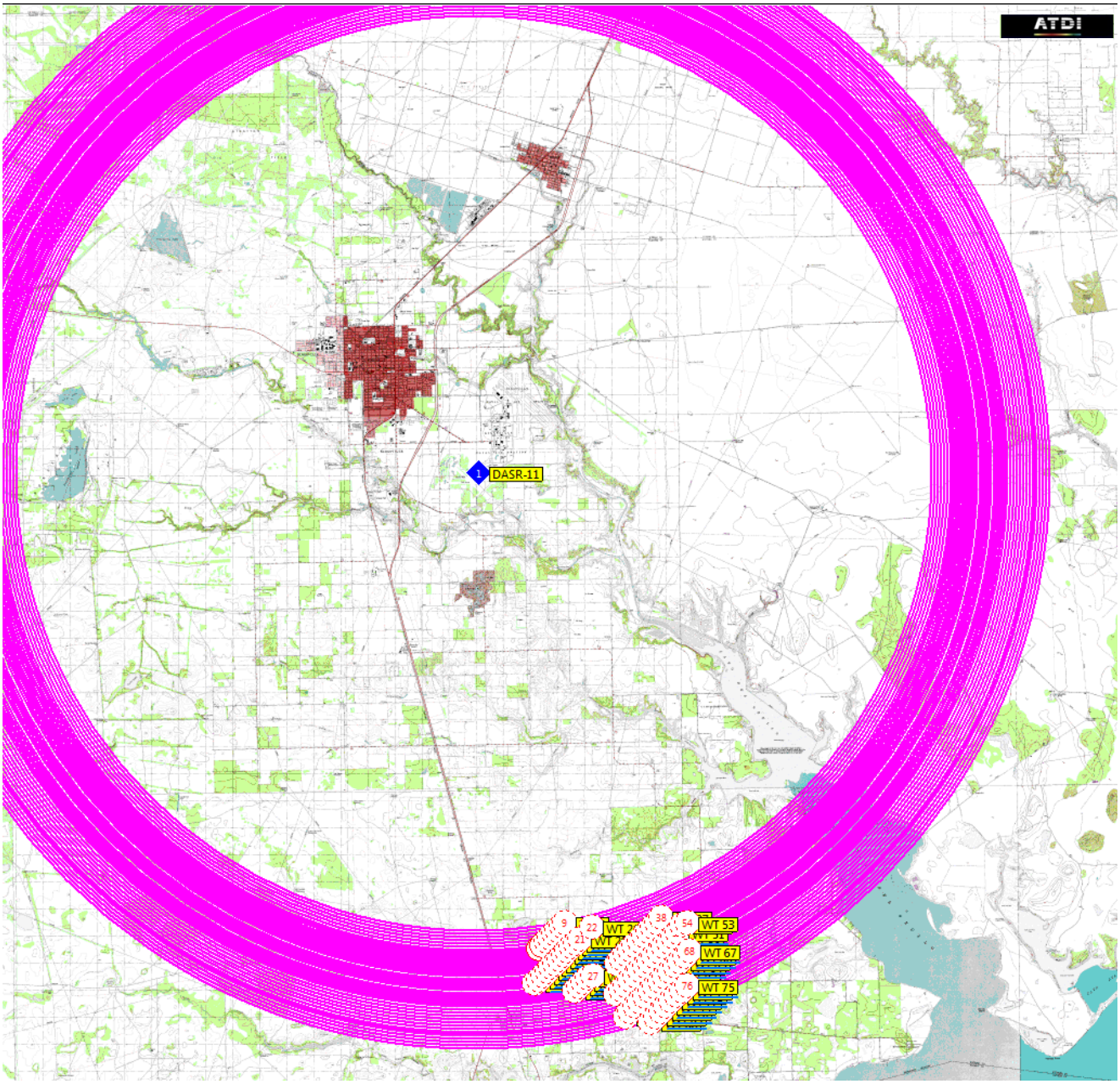

Figure 20: Rings of possible false target plots

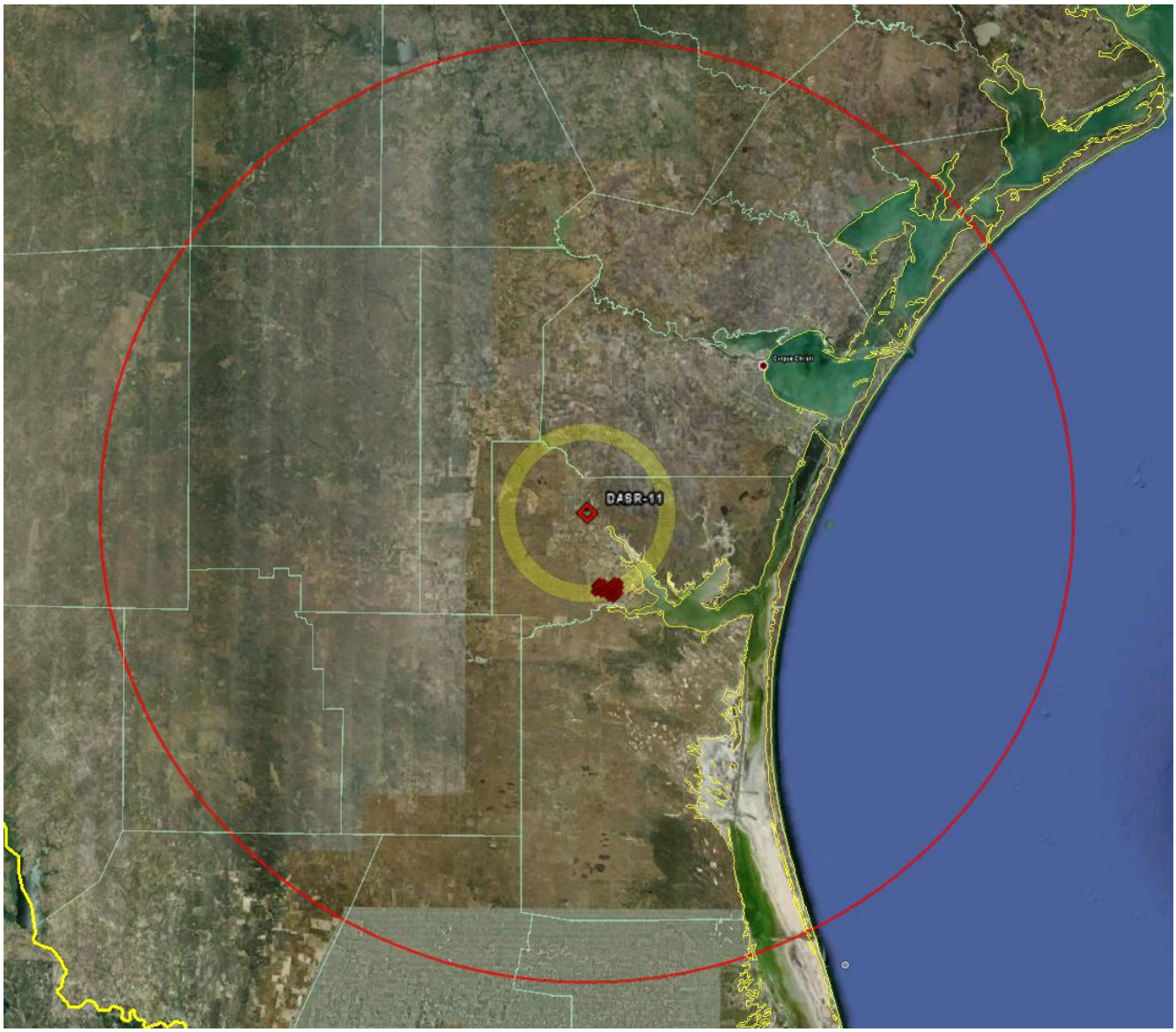

Figure 21: 60 nautical mile detection range of PSR

Both the low beam and the high beam are likely to see the creation of false target plots within a resolution cell that contains a wind turbine. For those cells, the power returns from the wind turbines are also likely to dominate the power returns from aircraft targets, causing possible target loss. The possibility of false target creation is relatively low for the high beam at any azimuth other than the radar's main beam. Due to the higher gain of the low beam at lesser elevations, though, false targets can be generated at almost any point on the concentric rings shown in the previous figures. Turbines must be located further away from the radar for the potential for false target plots to diminish. At a

distance of 25 nautical miles away from the radar, false target plots can potentially appear only when the wind farm is illuminated by the radar's main beam and in a 40 degree azimuth swath when the turbines are illuminated by the more powerful of the two main side lobes. As long as the turbines are within the line of sight of the radar, they can potentially create false target reports when they are illuminated by the main beam or the more powerful of the two main side lobes.

7. Conclusion

Ultimately, with the assumptions made and through both the mathematical models and the simulation results yielded by HTZ Warfare, potential interference effects caused by the Riviera wind farm are predicted. All 75 wind turbines are to be located within the 38 nautical mile radius of the radar's line-of-sight field, causing shadow regions. These shadow regions, though, are relatively small and should not cause target loss given the mandated flight paths around NAS Kingsville.

Due to modern processing techniques and increased levels of resolution, the clutter returns from wind turbines are not significant from the perspective of geographical footprint. Any single turbine in the wind farm will dominate the resolution cell it is in, potentially resulting in the target loss of an aircraft occupying the same cell. Given nominal resolution cell sizes for 0.8 Pd (.125nmi in radial range and 2.5° in azimuth swath), approximately 47 resolution cells are affected directly out of nearly 70,000 cells given the 60 nautical mile range of the PSR, while a further 67 are potentially affected as well due to their azimuth proximity to cells containing wind turbines. This means 0.17% of resolution cells are affected, .057% by total area. For a circular perimeter of radius 12 nautical miles that encompasses the Riviera wind farm in its entirety, 0.8% of resolution cells are effected, 1.42% by area.

Furthermore, due to the number of wind turbines and their potential clutter returns to the radar, a ring of minimum radius 9 nmi and maximum radius 11.5 nmi from the radar is created where false plots may be generated. Called the 'twinkling' effect, it is a direct result of the Doppler shifts imparted on power returned to the radar and the linear organization of the wind farm.

Ultimately, the questions of 'how many wind turbines are permissible' and 'how close is too close' are determined by the operational needs at the affected radar site and the mitigation capabilities allowed by the installed radar system. The number of wind turbines closely correlates to the number of resolution cells affected, where turbine reflected energy signatures dominate those of target aircraft within a cell. The potential for false targets diminishes as turbines are moved further away from radar. At approximately 25 nautical miles from the radar, there is little potential for false target generation in any azimuth other than the main beam and a side lobe.

Though this report covers shadowing, target loss, and false target generation effects, further radar performance degradation is possible. Multiple signal scatterings and overall noise level elevation (effects that are nearly impossible to summarized quantitatively) in the area of the wind farm can potentially harm the performance of the radar further. Since direct numerical calculations for these effects are not possible given their uncertainty, they were not covered in this report.

8. References

[1] Jackson, C.A.; Butler, M.M., "Options for mitigation of the effects of windfarms on radar sytems," *2007 IET International Conference on Radar Systems, 2007*, pp.1-6, 15-18 Oct 2007.

[2] Sergey, L.; Hubbard, O.; Zhen Ding; Ghadaki, H.; Jian Wang; Ponsford, T., "Advanced mitigating techniques to remove the effects of wind turbines and wind farms on primary surveillance radars," *IEEE Radar Conference, 2008*, pp.1-6, 26-30 May 2008.

[3] Department for Business Enterprise & Regulatory Reform, "Stealth Technology for Wind Turbines," Dec 2007.

[4] Drake, P.R.; Lok, Y.F., "Raytheon Wind Farm Mitigation Update", 21 Oct 2009.

[5] Bacon, D.F., "A proposed method for establishing an exclusion zone around a terrestrial fixed radio link outside of which a wind turbine will cause negligible degradation of the radio link performance," *Radiocommunications Agency UK Report*, Ver 1.1, 28 Oct 2002.

[6] Theil, A.; van Ewijk, L.J., "Radar Performance Degredation due to the Presence of Wind Turbines," *2007 IEEE Radar Conference*, pp.75-80, 17-20 Apr 2007.

[7] European Organisation for the Safety of Air Navigation, "Wind farm impact assessment techniques and mitigation measures," May 2007.

[8] Lemmon, J.J.; Carroll, J.E.; Sanders, F.H.; Turner, D., "Assessment of the Effects of Wind Turbines on Air Traffic Control Radars," *NTIA Technical Report TR-08-454*, July 2008.

[9] Greving, G.; Biermann, W.-D.; Mundt, R., "On the relevance of the measured or calculated RCS for objects on the ground - case wind turbines," *3rd European Conference on Antennas and Propagation, 2009*, pp.2216-2220, 23-27 March 2009.

[10] Civil Aviation Authority, "CAP 764: CAA Policy and Guidelines on Wind Turbines," Issue 1, July 2006.

[11]Kent, B.M.; Hill, K.C.; Buterbaugh, A.; Zelinski, G.; Hawley, R.; Cravens, L.; Tri-Van; Vogel, C.; Coveyou, T., "Dynamic Radar Cross Section and Radar Doppler Measurements of Commercial General Electric Windmill Power Turbines Part 1: Predicted and Measured Radar Signatures," *IEEE Antennas and Propagation Magazine*, vol. 50, no. 2, pp.211-219, Apr 2008.

[12] Civil Aviation Authority, “CAP 764: CAA Policy and Guidelines on Wind Turbines,” Issue 2, Feb 2009.

[13] Sanders, F.H.; Sole, R.L.; Bedford, B.L.; Franc, D.; Pawlowitz, T., “Effects of RF interference on radar receivers,” NTIA Report TR-06-444, Sept 2006.

[14] Poupart, G.J., “Wind Farms Impact on Radar Aviation Interests – Final Report,” Sept 2003.

[15] Spaven Consulting, “Wind Turbines and Radar: Operational Experience and Mitigation Measures,” Dec 2001.

[16] Ragheb, B., “Radar Signatures of Wind Turbines,” Jan 2009.

9. Appendix

A. Table of PSR clutter returns

Table 6: Comparison of PSR clutter returns of mathematical model and HTZ Warfare simulation

Turbine No.	*Distance (m)*	*Azimuth°*	*Clutter return- Mathematical model (dBm)*	*Clutter return- HTZ Warfare simulation (dBm)*
1	17771	172.79	-61.34	-61.34
2	17642	172.25	-61.21	-61.21
3	17522	171.73	-61.10	-61.09
4	17405	171.21	-60.98	-60.98
5	17289	170.68	-60.86	-60.86
6	17174	170.14	-60.75	-60.75
7	17051	169.59	-60.62	-60.62
8	16939	169.04	-60.51	-60.51
9	19026	173.66	-62.53	-62.53
10	18885	173.16	-62.40	-62.40
11	18754	172.65	-62.28	-62.28
12	18626	172.13	-62.16	-62.16
13	18498	171.61	-62.04	-62.04
14	18373	171.08	-61.92	-61.92
15	18249	170.54	-61.80	-61.80
16	18126	169.99	-61.68	-61.68
17	18005	169.44	-61.57	-61.57
18	17886	168.88	-61.45	-61.45
19	17759	168.3	-61.33	-61.33
20	17643	167.73	-61.22	-61.21
21	17308	165.96	-60.88	-60.88
22	19511	169.43	-62.96	-62.96
23	19384	168.88	-62.85	-62.85
24	19251	168.28	-62.73	-62.73
25	19128	167.71	-62.62	-62.62
26	19087	167.17	-62.58	-62.58
27	18859	164.25	-62.37	-62.37
28	18739	163.63	-62.26	-62.26
29	18625	162.99	-62.16	-62.16
30	18514	162.33	-62.05	-62.05
31	18411	161.7	-61.96	-61.95
32	18304	161.03	-61.85	-61.85

33	18200	160.35	-61.76	-61.75
34	18095	159.69	-61.65	-61.65
35	17996	159	-61.56	-61.56
36	17909	158.31	-61.48	-61.47
37	17811	157.63	-61.38	-61.38
38	19972	165.21	-63.37	-63.37
39	19845	164.57	-63.26	-63.26
40	19725	163.99	-63.15	-63.15
41	19606	163.31	-63.05	-63.05
42	19484	162.68	-62.94	-62.94
43	19367	162.01	-62.84	-62.83
44	19259	161.38	-62.74	-62.74
45	19147	160.69	-62.64	-62.63
46	19034	160.03	-62.53	-62.53
47	18937	159.34	-62.45	-62.44
48	18830	158.67	-62.35	-62.35
49	18730	157.95	-62.25	-62.25
50	18637	157.27	-62.17	-62.17
51	18542	156.55	-62.08	-62.08
52	18333	155.78	-61.88	-61.88
53	18366	155.11	-61.91	-61.91
54	20833	164.86	-64.10	-64.10
55	20707	164.25	-64.00	-64.00
56	20575	163.63	-63.89	-63.88
57	20457	162.97	-63.79	-63.78
58	20329	162.33	-63.68	-63.68
59	20214	161.69	-63.58	-63.58
60	20094	161.01	-63.48	-63.47
61	19975	160.34	-63.37	-63.37
62	19870	159.65	-63.28	-63.28
63	19756	158.97	-63.18	-63.18
64	19654	158.29	-63.09	-63.09
65	19550	157.57	-63.00	-63.00
66	19453	156.87	-62.91	-62.91
67	19355	156.14	-62.82	-62.82
68	21295	162.59	-64.48	-64.48
69	21163	161.94	-64.38	-64.37
70	21042	161.29	-64.28	-64.27
71	20925	160.63	-64.18	-64.18
72	20800	159.95	-64.08	-64.07
73	20692	159.25	-63.98	-63.98

74	20574	158.56	-63.89	-63.88
75	20468	157.87	-63.80	-63.79